Theory of velocity-dependent, collision-broadened, Doppler-free line shapes

M. J. O'Callaghan and J. Cooper
Joint Institute for Laboratory Astrophysics, University of Colorado and National Institute of Standards and Technology and Department of Physics, University of Colorado, Boulder, Colorado 80309-0440
(Received 9 December 1988)

Line-shape expressions for two-step resonant excitation in the presence of low-pressure perturbers are derived. These expressions allow for velocity-dependent broadening rates and are well suited for studying the line-shape contributions due to coherent excitation, incoherent excitation (due to dephasing collisions), interference between coherent and incoherent excitation, and velocity-changing collisions. Using the sodium $3S$-$3P$-$4D$ system perturbed by noble-gas atoms as an example and assuming C_6 interaction potentials, line shapes at a variety of laser detunings (Doppler selected atomic velocities) are numerically calculated to study variation in the line shape due to competing excitation paths and speed-dependent collision rates. In order to deal with both the line core and the line wing a composite collision kernel consisting of a Lorentzian kernel for small Δv_z collisions and a Keilson-Storer kernel for large Δv_z collisions is used. It is also demonstrated how the inelastic ($3P_{3/2}$-$3P_{1/2}$) velocity-changing collision kernel may be obtained from experimental data at low pressures. Theoretical line shapes and broadening rates are compared with experiment.

I. INTRODUCTION

Developments in the theory of two-photon–two-step pressure-broadened line shapes have made it possible, in principle, to extract information about both collisional velocity changes (VC) and collisional phase shifts (of the electronic wave functions) from experimentally observed line shapes. Due to the velocity-selective nature of the excitation process, it should also be possible to observe the speed dependence of both of these line-broadening mechanisms. However, the theoretical and experimental work to date has generally taken the approach of fitting specific collision models to observed line shapes rather than attempting an unprejudiced extraction of this fundamental information from the observations. Also, the speed dependence of the line broadening and the effect of small VC have largely been neglected. It is the purpose of this work, together with the accompanying experiment,[1] to study how these line-broadening mechanisms manifest themselves in the complete line shape and to demonstrate how these phase-shift and VC contributions may be isolated and measured.

The type of experiment of interest here is illustrated in Fig. 1. The atomic system consists of a ground state (state 0), two fine-structure states (states 1 and 2), and a final state (state 3). In the experiment of Ref. 1 these correspond to the Na $3S_{1/2}$, $3P_{1/2}$, $3P_{3/2}$, and $4D_{5/2}$ (or $4D_{3/2}$) states, respectively. Hyperfine structure as well as m degeneracy will be neglected. One single-mode cw laser (ω_1) excites atoms from state 0 to state 2 and a second laser (ω_2) is tuned to either the $1\rightarrow 3$ or $2\rightarrow 3$ transition with the state-3 population being monitored through either direct or cascade fluorescence.[1] ω_1 is tuned within the Doppler resonance line of the 0-2 transition, and only ground-state atoms whose velocity brings them into resonance with ω_1 will be excited; the "initial" state-2 velocity distribution will be quite narrow in the direction of the laser ($\hat{\mathbf{z}}$). In the absence of collisions the width Δv_z of the v_z distribution will be equivalent to the natural linewidth $\Delta\nu_z$ of the transition ($\Delta v_z/\lambda=\Delta\nu_n$). This is 10 MHz in the case of sodium, compared to the 1.7-GHz Doppler linewidth. In directions perpendicular to this axis the velocity distribution is still thermal (Maxwellian). The ω_2 laser beam is counter or copropagating with the ω_1 beam, so it excites this narrow state-2 v_z distribution to state 3 when the Doppler-shifted resonance condition is satisfied. However, this 2-3 transition has a natural width which also contributes to the ω_2 linewidth.

When perturbers are present collisions will redistribute and broaden this initial narrow v_z distribution and broaden the linewidths. The state-3 fluorescence line

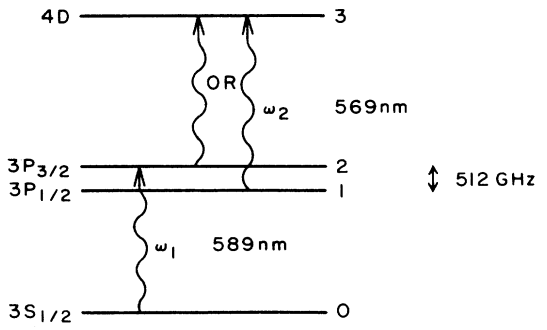

FIG. 1. Illustration of the atomic energy levels and transitions considered in this work.

shape, obtained by fixing ω_1 while scanning ω_2, maps out this state-2 v_z distribution, but with additional complexities due to line-broadening and coherence effects. Inelastic collisions will cause transitions between states 1 and 2 as well as VC, which will be detected in the ω_2 scan of the 1-3 transition. These VC collisions are characterized by a collision kernel[2-5] $W_{ij}(\mathbf{v}\rightarrow\mathbf{v}')$ which is the rate at which atoms in state i with velocity $\mathbf{v}$ are redistributed to state j with velocity v'.

Laser frequencies within many Doppler widths of line center are well within the impact limit,[6] and the effects of collisions on the electronic wave functions are well characterized as dephasing rates. When thermally averaged, these velocity-dependent broadening rates are the same as absorption or fluorescence line-broadening rates measured in the Lorentzian wings of pressure-broadened Voigt line shapes.

This resonant, two-frequency excitation process has already been studied both theoretically and experimentally.[2,3,5,7-10] With the exception of recent experimental work by Veza, Lawrenz, and Niemax[11] who used two-frequency excitation to study Ca line shapes broadened by Ne, the velocity dependence of collisional effects on such line shapes has not received much attention. As ω_1 is moved from the center of the Doppler line, where $\overline{v}_z=0$, into the Doppler wing the collision velocities increase. Since both the dephasing rates and collision kernels are v_z dependent[2,12] different linewidths and line shapes should be observed. In this work numerical line-shape calculations are performed to demonstrate speed-dependent effects. Another aspect that has not received much attention is the problem of determining collision kernels from observed line shapes. Previous work has instead concentrated on comparing observed line shapes with those calculated using simple collision models.[7,10] In addition, ω_2 line shapes have not been analyzed in the regions where both phase-shift broadening and velocity changes contribute. Here we develop low-pressure line-shape expressions in a form that facilitates determination of elastic and inelastic collision kernels as well as phase-shift broadening from experimental line shapes.

II. LINE-SHAPE EXPRESSIONS

Following Berman,[2,3,5] we use the density-matrix formalism to describe the four-level system (Fig. 1). The equation of motion for the density-matrix elements is

$$\dot{\rho}_{ij}(\mathbf{R},\mathbf{v},t)=-\mathbf{v}\cdot\nabla\rho_{ij}(\mathbf{R},\mathbf{v},t)-i\Omega_{ij}\rho_{ij}(\mathbf{R},\mathbf{v},t) -\tfrac{1}{2}(\gamma_i+\gamma_j)\rho_{ij}(\mathbf{R},\mathbf{v},t) +\frac{i}{\hbar}\langle i|[\mathbf{E}(t)\cdot e\mathbf{r},\rho]|j\rangle+[\dot{\rho}_{ij}(\mathbf{R},\mathbf{v},t)]_{\text{coll}} , \tag{1}$$

$$\mathbf{E}(t)=\mathbf{E}_1\cos(\mathbf{k}_i\cdot\mathbf{R}-\omega_1 t)+\mathbf{E}_2\cos(\mathbf{k}_i\cdot\mathbf{R}-\omega_2 t) . \tag{2}$$

Here $\Omega_{ij}=(E_i-E_j)/\hbar$, γ_i are the radiative decay rates, $[\dot{\rho}_{ij}]_{\text{coll}}$ represents the effect of collisions, and $\mathbf{E}(t)\cdot e\mathbf{r}$ represents the potential due to the radiation fields, where e is the electron's charge. $\mathbf{R}$ and $\mathbf{v}$ are the atomic coordinates and velocity while $\mathbf{r}$ are electronic coordinates.

As discussed in Sec. I, a typical experiment involves observing (through fluorescence) the total state-3 population. Accordingly, the goal here is to compute $\int\rho_{33}(\mathbf{v})d^3v$. Here ω_1 is tuned near the Ω_{20} resonance while ω_2 may be tuned near either Ω_{32} or Ω_{31}.

The collisional component of Eq. (1) $[\dot{\rho}_{ij}]_{\text{coll}}$ is written in terms of collision kernels[2,3,5] $W_{ij}(\mathbf{v}\rightarrow\mathbf{v}')$ which specify the probability of an atom in state i and moving with velocity $\mathbf{v}$ being scattered to state j with velocity $\mathbf{v}'$ plus terms which characterize the effect of dephasing collisions on the electronic wave functions. All of these terms are functions of quantum-mechanical differential scattering cross sections. The effect of collisions on diagonal density-matrix elements is

$$[\dot{\rho}_{ii}(\mathbf{R},\mathbf{v},t)]_{\text{coll}}=\sum_j\left[-\Gamma_{ij}(\mathbf{v})\rho_{ii}(\mathbf{R},\mathbf{v},t) +\int W_{ji}(\mathbf{v}'\rightarrow\mathbf{v}) \times\rho_{jj}(\mathbf{R},\mathbf{v}',t)d^3v'\right] , \tag{3}$$

where d^3v' indicates a volume integral over the space of $\mathbf{v}'$. The sum is over all states j which are connected to state i by collisions, due either to velocity changes (elastic collisions, $j=i$) or state-changing collisions (inelastic collisions, $j\neq i$). The loss rate $\Gamma_{ij}(\mathbf{v})$ from state i and velocity $\mathbf{v}$ to state j is related to the collision kernel by

$$\Gamma_{ij}(\mathbf{v})=\int W_{ij}(\mathbf{v}-\mathbf{v}')d^3v' . \tag{4}$$

The effect of collisions on off-diagonal matrix elements is more complex. In the limit that the perturber mass is much less than the active atom mass, or that the scattering functions in the two optically connected states are very different from one another, the following approximation may be used[2,3,12]:

$$[\dot{\rho}_{ij}]_{\text{coll}}=-[\gamma_{ij}^c(v)+i\delta_{ij}(v)]\rho_{ij},\quad i\neq j . \tag{5}$$

Here $\gamma_{ij}^c(v)$ and $\delta_{ij}(v)$ represent, respectively, a speed-dependent broadening and shift of the line due to collisions and $v=|\mathbf{v}|$. These terms are due to collisional dephasing and (when thermally averaged) are the same quantities obtained in studies of pressure broadening in the wings of Doppler lines.

Since we are interested only in the weak-field limit, we first solve Eq. (1) for states 0,1,2 under the influence of ω_1. These solutions are then used to solve for ρ_{33} in the presence of ω_2. The rotating wave approximation is used.[13] Since only steady-state solutions are of interest here, we make the following substitutions:

$$\rho_{20}(\mathbf{R},\mathbf{v},t)=\tilde{\rho}_{20}(\mathbf{v})e^{i(\mathbf{k}_1\cdot\mathbf{R}-\omega_1 t)} , \tag{6a}$$

$$\rho_{32}(\mathbf{R},\mathbf{v},t)=\tilde{\rho}_{32}(\mathbf{v})e^{i(\mathbf{k}_2\cdot\mathbf{R}-\omega_2 t)} , \tag{6b}$$

$$\rho_{30}(\mathbf{R},\mathbf{v},t)=\tilde{\rho}_{30}(\mathbf{v})e^{i[(\mathbf{k}_1+\mathbf{k}_2)\cdot\mathbf{R}-(\omega_1+\omega_2)t]} , \tag{6c}$$

$$\rho_{ii}(\mathbf{R},\mathbf{v},t)=\tilde{\rho}_{ii}(\mathbf{v}) . \tag{6d}$$

Assuming $\rho_{22}\ll\rho_{00}$, we see that the equations for states 0,1,2 become

$$(\gamma_2+\Gamma_2)\tilde{\rho}_{22}(\mathbf{v})=-\frac{1}{\hbar}\mathrm{Im}[V_{20}\tilde{\rho}_{02}(\mathbf{v})] + \int W_{22}(\mathbf{v}'\to\mathbf{v})\tilde{\rho}_{22}(\mathbf{v}')d^3v' + \int W_{12}(\mathbf{v}'\to\mathbf{v})\tilde{\rho}_{11}(\mathbf{v}')d^3v' , \quad (7a)$$

$$(\gamma_1+\Gamma_1)\tilde{\rho}_{11}(\mathbf{v})=\int W_{11}(\mathbf{v}'\to\mathbf{v})\tilde{\rho}_{11}(\mathbf{v}')d^3v' + \int W_{21}(\mathbf{v}'\to\mathbf{v})\tilde{\rho}_{22}(\mathbf{v}')d^3v' , \quad (7b)$$

$$\tilde{\rho}_{00}(\mathbf{v})=(\pi u^2)^{-3/2}e^{-(v/u)^2},\quad u=(2kT/m)^{1/2} , \quad (7c)$$

$$(\tilde{\Delta}_{20}+i\gamma_{20})\tilde{\rho}_{20}(\mathbf{v})=-\frac{V_{20}}{2\hbar}\tilde{\rho}_{00}(\mathbf{v}) , \quad (7d)$$

$$\gamma_{ij}=\tfrac{1}{2}(\gamma_i+\gamma_j)+\gamma_{ij}^c(\mathbf{v}) , \quad (7e)$$

$$\Gamma_1=\Gamma_{11}(v)+\Gamma_{12}(v) , \quad (7f)$$

$$\Gamma_2=\Gamma_{22}(v)+\Gamma_{21}(v) , \quad (7g)$$

$$\tilde{\Delta}_{20}=\Delta_{20}-\mathbf{k}_1\cdot\mathbf{v},\quad \Delta_{20}=\omega_1-\Omega_{20}-\delta_{20}(v) , \quad (7h)$$

$$V_{20}=\langle 2|\mathbf{E}_1\cdot\mathbf{r}|0\rangle . \quad (7i)$$

Note that even though the terms defined in Eqs. (7e) through (7h) are functions of $\mathbf{v}$ they are written, e.g., as Γ rather than $\Gamma(\mathbf{v})$. This is done in order to keep subsequent expressions from becoming too cumbersome.

It has been assumed that ω_1 is weak enough such that $\tilde{\rho}_{00}$ is unchanged from its equilibrium distribution. In this limit Eq. (7d) is solved for $\tilde{\rho}_{02}$ and the following expressions for $\tilde{\rho}_{11}$ and $\tilde{\rho}_{22}$ are then obtained from Eqs. (7a) and (7b):

$$\tilde{\rho}_{22}(\mathbf{v})=L_{22}(\mathbf{v})+U_{21}\tilde{\rho}_{11}(\mathbf{v})+U_{22}\tilde{\rho}_{22}(\mathbf{v}) , \quad (8a)$$

$$\tilde{\rho}_{11}(\mathbf{v})=U_{12}\tilde{\rho}_{22}(\mathbf{v})+U_{11}\tilde{\rho}_{11}(\mathbf{v}) , \quad (8b)$$

$$L_{22}(\mathbf{v})=\frac{|V_{20}|^2}{2\hbar^2(\gamma_2+\Gamma_2)}\frac{\gamma_{20}}{\tilde{\Delta}_{20}^2+\gamma_{20}^2}\tilde{\rho}_{00}(\mathbf{v}) , \quad (8c)$$

$$U_{ij}\tilde{\rho}_{jj}(\mathbf{v})=\frac{1}{\gamma_i+\Gamma_i}\int W_{ji}(\mathbf{v}'\to\mathbf{v})\tilde{\rho}_{jj}(\mathbf{v}')d^3v' . \quad (8d)$$

$L_{22}(\mathbf{v})$ is in effect the state-2 velocity distribution initially produced by the ω_1 radiation before velocity-changing collisions occur. The operators U_{ij} represent velocity-changing collisions which take a state-j velocity distribution $\tilde{\rho}_{jj}(\mathbf{v})$ and transform it to a state-i distribution $\tilde{\rho}'_{ii}(\mathbf{v})=U_{ij}\tilde{\rho}_{jj}(\mathbf{v})$. It is important to note that the order of the i,j subscripts used for the U_{ij} operators is opposite that which is used for the kernels W_{ji} [note Eq. (8d)]. The reason for this will be evident below in Eqs. (9) and (10). A solution of Eq. (8b) may be written as an infinite series[14] of products of the U_{ij} operators

$$\tilde{\rho}_{11}(\mathbf{v})=\sum_{n=0}^{\infty}U_{11}^nU_{12}\tilde{\rho}_{22}(\mathbf{v}) . \quad (9)$$

Using this solution in Eq. (8a) and using the subsequent solution for $\tilde{\rho}_{22}$ in Eq. (9), we obtain

$$\begin{aligned}\tilde{\rho}_{22}(\mathbf{v})&=\sum_{m=0}^{\infty}\left[U_{22}+U_{21}\sum_{n=0}^{\infty}U_{11}^nU_{12}\right]^mL_{22}(\mathbf{v})\\&=[1+U_{22}+(U_{22}^2+U_{21}U_{12})+\cdots]L_{22}(\mathbf{v})\\&=(1+F_{22})L_{22}(\mathbf{v}) ,\end{aligned} \quad (10a)$$

$$\begin{aligned}\tilde{\rho}_{11}(\mathbf{v})&=\sum_{n=0}^{\infty}U_{11}^nU_{12}\sum_{m=0}^{\infty}\left[U_{22}+U_{21}\sum_{l=0}^{\infty}U_{11}^lU_{12}\right]^mL_{22}(\mathbf{v})\\&=F_{12}L_{22}(\mathbf{v}) .\end{aligned} \quad (10b)$$

The sum of operators in Eq. (10a), defined as F_{22}, represents all of the possible collision sequences which begin and end in state 2, while Eq. (10b) contains all of the possible collision sequences, defined as F_{12}, which begin in state 2 and end in state 1.

In solving for ρ_{33} there are two cases to consider: $\omega_2\approx\Omega_{32}$ and $\omega_2\approx\Omega_{31}$. In the first case the equations for the final density-matrix elements (using the same substitutions and definitions as before) become

$$\gamma_3\tilde{\rho}_{33}=-\frac{1}{\hbar}\mathrm{Im}(V_{32}\tilde{\rho}_{23})-\Gamma_3\tilde{\rho}_{33} + \int W_{33}(\mathbf{v}'\to\mathbf{v})\tilde{\rho}_{33}(\mathbf{v}')d^3v' , \quad (11a)$$

$$(\tilde{\Delta}_{32}+i\gamma_{32})\tilde{\rho}_{32}=-\frac{1}{2\hbar}V_{32}\tilde{\rho}_{22}+\frac{1}{2\hbar}\tilde{\rho}_{30}V_{02} , \quad (11b)$$

$$(\tilde{\Delta}_{30}+i\gamma_{30})\tilde{\rho}_{30}=-\frac{1}{2\hbar}V_{32}\tilde{\rho}_{20} , \quad (11c)$$

$$\tilde{\Delta}_{32}=\Delta_{32}-\mathbf{k}_2\cdot\mathbf{v},\quad \Delta_{32}=\omega_2-\Omega_{32}-\delta_{32} , \quad (11d)$$

$$\tilde{\Delta}_{30}=\Delta_{30}-(\mathbf{k}_1+\mathbf{k}_2)\cdot\mathbf{v},\quad \Delta_{30}=(\omega_1+\omega_2)-\Omega_{30}-\delta_{30} , \quad (11e)$$

$$V_{32}=\langle 3|\mathbf{E}_2\cdot\mathbf{r}|2\rangle , \quad (11f)$$

$$\Gamma_3=\Gamma_{33}(\mathbf{v}) . \quad (11g)$$

We have made the weak-field approximations $\tilde{\rho}_{33}\ll\tilde{\rho}_{22}$ and $\tilde{\rho}_{32}\ll\tilde{\rho}_{20}$. Combining Eqs. (11b) and (11c) with Eqs. (7d) and (10a), $\tilde{\rho}_{32}$ is obtained,

$$\tilde{\rho}_{32}=\frac{V_{32}|V_{20}|^2}{8\hbar^3}\left[\left[\frac{2}{\gamma_2+\Gamma_2}\frac{\gamma_{20}}{\tilde{\Delta}_{20}^2+\gamma_{20}^2}-\frac{1}{\tilde{\Delta}_{20}+i\gamma_{20}}\frac{1}{\tilde{\Delta}_{30}+i\gamma_{30}}\right]\frac{\tilde{\rho}_{00}}{\tilde{\Delta}_{32}+i\gamma_{32}} + \frac{2}{\tilde{\Delta}_{32}+i\gamma_{32}}F_{22}\left[\frac{1}{\gamma_2+\Gamma_2}\frac{\gamma_{20}}{\tilde{\Delta}_{20}^2+\gamma_{20}^2}\tilde{\rho}_{00}\right]\right] . \quad (12)$$

Before using Eq. (12) in Eq. (11a) recall that what is measured is $\int \tilde{\rho}_{33}(\mathbf{v})d^3v$. When performing this integration the collisional terms of Eq. (11a) add to zero, i.e., velocity-changing collisions (within state 3) cannot alter the total state-3 population. The line-shape expression is then (for $\omega_2 \approx \Omega_{32}$)

$$\rho_{33}^{\mathrm{el}}(\omega_1,\omega_2)=\frac{|V_{32}|^2|V_{20}|^2}{8\hbar^4\gamma_3}\int\left[\left[\frac{\gamma_{30}}{(\tilde{\Delta}_{20}^2+\gamma_{20}^2)(\tilde{\Delta}_{30}^2+\gamma_{30}^2)}+\frac{2\gamma_{20}^c-\Gamma_2}{\gamma_2+\Gamma_2}\frac{\gamma_{32}}{(\tilde{\Delta}_{20}^2+\gamma_{20}^2)(\tilde{\Delta}_{32}^2+\gamma_{32}^2)}\right.\right.$$
$$\left.+\frac{(\gamma_{32}^c-\gamma_{30}^c-\gamma_{20}^c)(\tilde{\Delta}_{32}\tilde{\Delta}_{30}-\gamma_{32}\gamma_{30})+(\delta_{30}-\delta_{20}-\delta_{32})(\gamma_{32}\tilde{\Delta}_{30}+\gamma_{30}\tilde{\Delta}_{32})}{(\tilde{\Delta}_{20}^2+\gamma_{20}^2)(\tilde{\Delta}_{32}^2+\gamma_{32}^2)(\tilde{\Delta}_{30}^2+\gamma_{30}^2)}\right]\rho_{00}$$
$$\left.+\frac{2\gamma_{32}}{\tilde{\Delta}_{32}^2+\gamma_{32}^2}F_{22}\left[\frac{1}{\gamma_2+\Gamma_2}\frac{\gamma_{20}}{\tilde{\Delta}_{20}^2+\gamma_{20}^2}\rho_{00}\right]\right]d^3v\ . \tag{13}$$

The first integrand of Eq. (13) is present even in the absence of collisions and shall be referred to as the "coherent" term. The second integrand is due to phase-disrupting collisions without velocity changes, and is referred to as the "incoherent" term, while the third integrand ("interference" term) is due to interference between the coherent and incoherent excitation processes. The final term, containing the F_{22} operator, contains the effect of velocity-changing and $(2\leftrightarrow 1)$ state-changing collisions. Since the excitation process leading to Eq. (13) does not require the presence of $(2\leftrightarrow 1)$ inelastic collisions we refer to it as the elastic line shape and hence designate it as ρ^{el}.

For the second case $(\omega_2 \approx \Omega_{31})$ the line-shape expression is

$$\rho_{33}^{\mathrm{in}}(\omega_1,\omega_2)=\frac{|V_{31}|^2|V_{20}|^2}{4\hbar^4\gamma_3}\int\frac{\gamma_{31}}{\tilde{\Delta}_{31}^2+\gamma_{31}^2}F_{12}\left[\frac{1}{\gamma_2+\Gamma_2}\frac{\gamma_{20}}{\tilde{\Delta}_{20}^2+\gamma_{20}^2}\rho_{00}\right]d^3v\ . \tag{14}$$

As compared to $\rho_{33}^{\mathrm{el}}(\omega_1,\omega_2)$ this line-shape expression contains only terms due to velocity- and state-changing collisions (through the operator F_{12}). This results from the fact that all inelastic collisions disrupt the phase, leaving only the incoherent term. Since it is due to the excitation process $0\rightarrow 2\rightarrow(\text{collision})\rightarrow 1\rightarrow 3$, we refer to it as the inelastic line shape.

III. COLLISION KERNELS

As noted earlier, the initial state-2 velocity distribution $L_{22}(\mathbf{v})$ is thermal in directions transverse to $\mathbf{k}_1$ and effectively Lorentzian in the direction parallel to $\mathbf{k}_1$ (due to velocity-selective excitation by ω_1). Defining a $\hat{\mathbf{z}}$ axis such that $\mathbf{k}_1=k_1\hat{\mathbf{z}}$ we adopt the approximation $\rho_{ii}(\mathbf{v})=\rho_{ii}(\mathbf{v}_t)\rho_{ii}(v_z)$, where $\mathbf{v}_t$ are velocity components transverse to the z axis. It is assumed that to lowest-order collisions affect $\rho_{ii}(v_z)$ but not the thermal $\rho_{ii}(\mathbf{v}_t)$. Accordingly a one-dimensional kernal is defined such that

$$\int W_{ii}(\mathbf{v}'-\mathbf{v})\rho_{ii}(\mathbf{v}')d^3v'$$
$$=\rho_{ii}(\mathbf{v}_t)\int W_{ii}(v_z'\rightarrow v_2)\rho_{ii}(v_z')dv_z'\ .$$

This, in turn, requires

$$W_{ii}(v_z'\rightarrow v_z)=\rho_{ii}^{-1}(\mathbf{v}_t)\int W_{ii}(\mathbf{v}'\rightarrow\mathbf{v})\rho_{ii}(\mathbf{v}_t')d^2v_t'\ . \tag{15}$$

In the velocity-changing components of the line-shape expressions [Eqs. (13) and (14)] we make the simplifying approximation of replacing the various velocity dependent $\gamma(v),\Gamma(v)$ by appropriately averaged values $\bar{\gamma},\bar{\Gamma}$. These are taken to be constants in the v_z integrations below, but they depend on Δ_{20} as this determines the center of the initially excited v_z distribution. In essence, we assume correctly that the initial v_z distribution is sharply peaked. This will be discussed further in Secs. IV and V. With these approximations the line-shape expression ρ_{33}^{in} [Eq. (14)] and the velocity-changing part of ρ_{33}^{el} [Eq. (13)] become

$$(\rho_{33}^{\mathrm{el}})_{\mathrm{VC}}=\frac{|V_{32}|^2|V_{20}|^2}{4\hbar^4\gamma_3}\frac{1}{\gamma_2+\bar{\Gamma}_2}$$
$$\times\int\frac{\bar{\gamma}_{32}}{\tilde{\Delta}_{32}^2+\bar{\gamma}_{32}^2}F_{22}'\left[\frac{\bar{\gamma}_{20}}{\tilde{\Delta}_{20}^2+\bar{\gamma}_{20}^2}\rho_{00}(v_z)\right]dv_z\ , \tag{16a}$$

$$F_{22}'=U_{22}'+(U_{22}'^2+U_{21}'U_{12}')+\cdots\ , \tag{16b}$$

$$\rho_{33}^{\mathrm{in}}=\frac{|V_{31}|^2|V_{20}|^2}{4\hbar^4\gamma_3}\frac{1}{\gamma_2+\bar{\Gamma}_2}$$
$$\times\int\frac{\bar{\gamma}_{31}}{\tilde{\Delta}_{31}^2+\bar{\gamma}_{31}^2}F_{12}'\left[\frac{\bar{\gamma}_{20}}{\tilde{\Delta}_{20}^2+\bar{\gamma}_{20}^2}\rho_{00}(v_z)\right]dv_z\ , \tag{16c}$$

$$F_{12}'=U_{12}'+(U_{12}'U_{22}'+U_{11}'U_{12}')+\cdots\ , \tag{16d}$$

$$U_{ij}'\rho_{jj}(v_z)=\frac{1}{\gamma_i+\bar{\Gamma}_i}\int W_{ji}(v_z'\rightarrow v_z)\rho_{jj}(v_z')dv_z'\ . \tag{16e}$$

The transverse velocity integrals have been performed in order to arrive at expressions which are now in terms of one-dimensional collision kernels. The primes on the U',F' operators are used to distinguish these one-dimensional operators $(v_z\rightarrow v_z')$ from U,F operators which act in three dimensions $(\mathbf{v}\rightarrow\mathbf{v}')$.

In order to use these line-shape expressions the kernels must be known. Calculating kernels for realistic interatomic forces is a difficult task. Due to their relative computational simplicity the Keilson-Storer kernel and one

derived for hard-sphere scattering have commonly been used.[2,3,7,10] In experiments performed by Laio *et al.*,[7] which were at perturber densities where several collisions occur during a radiative lifetime, it was concluded that either Keilson-Storer or hard-sphere models produced reasonable agreement with experiment in the line-wing region corresponding to large VC, with the hard-sphere kernel producing the best results for the heavier perturbers. However, agreement near the resonance, corresponding to small velocity changes, was poor. Haverkort *et al.*[10] have successfully used a composite Keilson-Storer kernel to fit their results under similar conditions while studying both elastic and inelastic collisions.

Ho and Chu[15] have calculated collision kernels for Ar-Ar collisions and Na(3*s*)-Ar collisions assuming a C_6 potential. The kernels they arrived at were qualitatively similar to the Keilson-Storer or hard-sphere kernel for large Δv_z but substantially different for small Δv_z. For computational simplicity we choose to represent this type of behavior with a narrow Lorentzian, which describes small-Δv_z collisions, plus a Keilson-Storer kernel which describes large-Δv_z collisions,

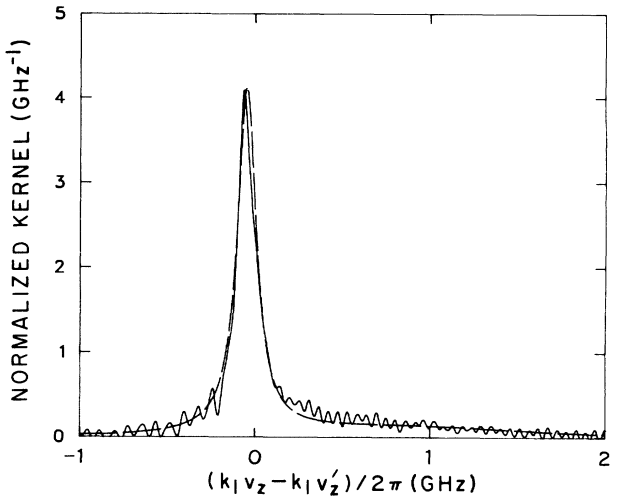

FIG. 3. Comparison of the inelastic kernel, —— (Na $3P_{3/2}\rightarrow 3P_{1/2}$ caused by Ar) determined in the experiment of Ref. 1 to a phenomenological kernel, — — —, of the type given in Eq. (17). See text for details.

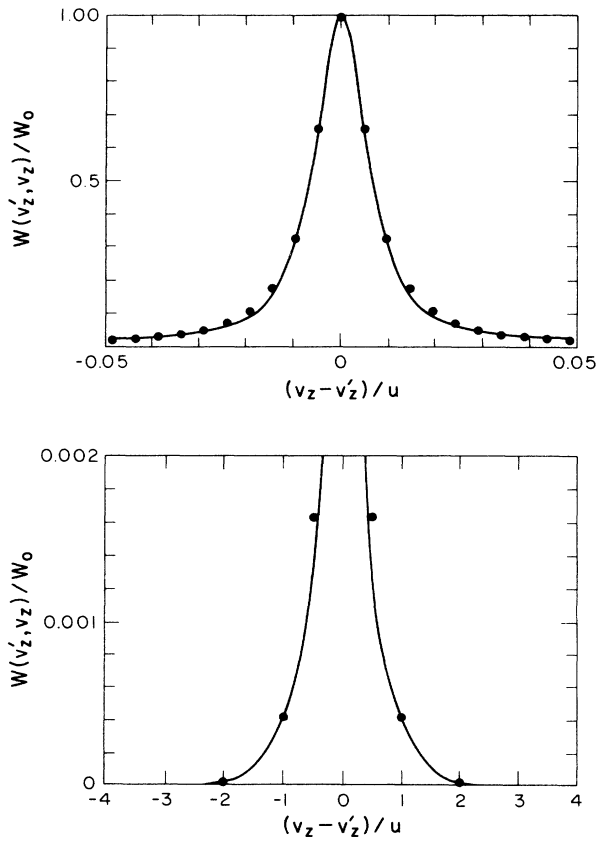

FIG. 2. Comparison of Ho and Chu's Na(3*S*)-Ar kernel for $v_z=0$, —— to one composed of a Lorentzian plus a Keilson-Storer, ●.

$$W_{ij}(v_z'\rightarrow v_z)=\bar{\Gamma}_{ij}(v_z')\left[\frac{A}{\pi}\frac{w}{(v_z'-v_z)^2+w^2}+B\left[\frac{1}{\pi\Delta u^2}\right]^{1/2}\times e^{-(v_z-\alpha v_z')^2/(\Delta u)^2}\right], \quad (17a)$$

$$\Delta u=(1-\alpha^2)^{1/2}u\ . \quad (17b)$$

Here α (<1) is a parameter that depends on the perturber-emitter mass ratio and A,B determine the relative contributions of the two normalized component kernels $A+B=1$. The Na(3*s*)-Ar kernel of Ho and Chu (for $v_z'=0$) is compared to this composite kernel in Fig. 2 for $\Delta_{20}=0.0$. Here we used $A=0.924$, $B=0.076$, $\alpha=0.2$, and the full width at half maximum (FWHM) of the kernel is $0.0135u$, which corresponds to 9 MHz at the temperature (300 K) used for Ho and Chu's calculation. These values were obtained by fitting the kernel of Eq. (17) to the kernel of Ho and Chu. The value of α agrees with that expected for Na-Ar collisions.[2]

In Ref. 1 the inelastic kernel $W_{21}(v_z\rightarrow v_z')$ has been determined from experiment for Na perturbed by Ar. Having replaced v_z,v_z' by k_1v_z,k_1v_z' (where $k_1=\omega_1/c$), this experimentally determined kernel is compared to the composite kernel of Eq. (17) in Fig. 3. The parameters used for the composite kernel are $A=0.8$, $B=0.2$, $\alpha=0.2$, and $k_1w/2\pi=125$ MHz. The kernels have been aligned so that their centers (defined at their half heights) are coincident and their areas have been normalized to 1. It can be seen from Fig. 3 that the small Δv_z part of the experimentally determined kernel exhibits an asymmetry not found in the Lorentzian part of Eq. (17). However, the discrepancies between these two kernels are small

enough that Eq. (17) represents a very good approximation to the actual kernel.

IV. LIMITING CASES

Before presenting the results from numerical evaluation of Eqs. (13) and (14), it is useful to examine simple limiting cases where some of the line-shape components may be evaluated analytically. First of all we will make estimates of $\overline{\gamma}$, etc., using the initial excited-state velocity distribution $\rho_{22}(\mathbf{v})$ calculated on the assumption (good to lowest order) that subsequent velocity-changing collisions are unimportant. We will then evaluate ρ_{33} for different $\tilde{\Delta}_{20}$ using simplified collision kernels.

A. Average collisional rates

The line-broadening coefficient γ is proportional to $\langle v_r \rangle^{3/5}$ for C_6 potentials, where v_r is the relative velocity. For a Maxwellian velocity distribution the difference between $\langle v^{3/5} \rangle$ and $\langle v_{\rm av} \rangle^{3/5}$, where $v_{\rm av}=(\langle v_r \rangle^2)^{1/2}$ is less than 10%. This minor difference is due to the peaked nature of the velocity distribution. We will assume that a similarly small error is made by using $v_{\rm av}$ for the collisionally modified distribution which will also be strongly peaked about some (different) value of $v_{\rm av}$. Since the C_6 broadening coefficient also varies as $T^{0.3}$ it will be convenient to define an effective temperature $T_{\rm eff} \propto v_{\rm av}^2$ such that $\overline{\gamma} \propto T_{\rm eff}^{0.3}$. In order to arrive at an approximate expression for $T_{\rm eff}$ we must evaluate the following integral:

$$\tfrac{3}{2}kT_{\rm eff}=\tfrac{1}{2}\mu \int\int |\mathbf{v}-\mathbf{v}_p|^2 f(\mathbf{v}) f_p(\mathbf{v}_p) d^3v\, d^3v_p \ . \tag{18}$$

This is the average center-of-mass kinetic energy of the collisions where μ is the reduced mass, $f(\mathbf{v})$ the active atom velocity distribution, and $f_p(\mathbf{v}_p)$ the (Maxwellian) perturber velocity distribution. We approximate the state-2 velocity distribution $f(\mathbf{v})$ to be proportional to the following highly peaked distribution:

$$\tilde{\rho}_{22}(\mathbf{v})=\frac{\pi |V_{20}|^2}{\hbar^2(\gamma_2+\Gamma_2)} \delta(v_z-\Delta_{20}/k_1)(\pi u^2)^{-3/2} e^{-(v/u)^2} \ . \tag{19}$$

This is the lowest-order term of Eq. (10a) in which the narrow (relative to the Maxwellian distribution) Lorentzian has been replaced by a δ function, and the velocity redistribution terms U_{ij} have been dropped. Using the distribution of Eq. (19) (after being normalized) the integral of Eq. (18) is evaluated to obtain an expression for $T_{\rm eff}$,

$$T_{\rm eff}=T\mu\{(1/m_p)+(1/m)(\tfrac{2}{3})[1+(\Delta_{20}/\Omega_D)^2 \ln 2]\} \ . \tag{20}$$

Here $\Omega_D=(\ln 2)^{1/2}k_1 u$ is the HWHM of the Doppler line, and u is the most probable thermal speed as given by Eq. (7c). As stressed earlier, for this to be valid, the velocity distribution must be sharply peaked about a $v_{\rm av}$. At $|\Delta_{20}/\Omega_D|=0.424$ we have $T_{\rm eff}=T$. At approximately this detuning we expect $\overline{\gamma}(\Delta_{20})=\gamma_{\rm th}$, where $\gamma_{\rm th}$ is the thermally averaged broadening coefficient obtained in traditional measurements of pressure broadening of the Lorentzian wing of Voigt line shapes. It will be shown that numerical evaluation of Eq. (13) produces the expected $T_{\rm eff}^{0.3}$ dependence and so supports the validity of these simple approximations.

B. $\Delta_{20} \ll \Omega_D$

The first limiting case of Eq. (13) we shall consider is for $\Delta_{20} \ll \Omega_D$, Ω_D being the Doppler HWHM. When the various γ, Γ are replaced by their averaged (dependent on Δ_{20}) values $\overline{\gamma}, \overline{\Gamma}$, the coherent, incoherent, and interference integrands depend only on v_z, so the $dv_x dv_y$ integrals are easy to perform. Making use of the v_z selectivity of excitation due to ω_1 (i.e., by using the δ function), we replace $\tilde{\rho}_{00}(v_z)$ of Eq. (13) by

$$(\pi u^2)^{-1/2} \exp[-(\Delta_{20}/k_1 u)^2]$$

and remove it from the integral. The coherent and incoherent terms are now convolutions of Lorentzians. These are easily evaluated since the convolution of two Lorentzians produces a Lorentzian. The interference term is much more complex and will not be evaluated here. As will be seen in Sec. V, when numerical calculations are performed (using Na-Ar broadening as an example) the interference term is much smaller than the coherent and incoherent terms but can nevertheless have a significant effect on the width of the line. We will take the limiting case of the kernel of Eq. (17) in which the width of the Lorentzian part approaches zero and inelastic collisions are neglected so $\overline{\Gamma}_2=\overline{\Gamma}_{22}$ (see Sec. V for further discussion). In this limit the Lorentzian kernel is replaced by a δ function

$$W_{22}(v_z-v_z')=\overline{\Gamma}_{22}[A\delta(v_z-v_z')+BW_K(v_z \to v_z')] \ , \tag{21a}$$

$$A+B=1$$

$$U_{22}\rho(v_z)=\frac{\overline{\Gamma}_2}{\gamma_2+\overline{\Gamma}_2}\left[A\rho+B\int W_K(v_z' \to v_z)\rho(v_z')dv_z'\right] \ , \tag{21b}$$

$$\int W_K(v_z \to v_z')dv_z'=1 \ . \tag{21c}$$

Here $W_K(v_z \to v_z')$ is the Keilson-Storer part of Eq. (17). In this approximation the collision operator F_{22} [Eq. (16b)] becomes (see the Appendix)

$$F_{22}'=\frac{1}{\gamma_2+B\overline{\Gamma}_2}\left[A\overline{\Gamma}_2+(\gamma_2+\overline{\Gamma}_2) \times \sum_{n=1}^{\infty}\left[\frac{B\overline{\Gamma}_2}{\gamma_2+B\overline{\Gamma}_2}\right]^n W_{\rm KSO}^n\right] \ , \tag{22a}$$

$$W_{\rm KSO}\rho=\int W_K(v_z' \to v_z)\rho(v_z')dv_z' \ . \tag{22b}$$

Here $W_{\rm KSO}$ is an integral operator which represents the effect of single collisions using a Keilson-Storer kernel. When Eq. (22a) is inserted into the line-shape expression Eq. (13), and using Eq. (16a) for the velocity-changing component, the first term ($A\overline{\Gamma}_{22}$) of F_{22}' simply introduces a constant times the Lorentzians in Δ_{20} and Δ_{32}. This term and the incoherent term are proportional to one another and can be combined. Making use of the ap-

proximation that the large-Δv_z part of the velocity-changing kernel varies slowly compared to the widths $\gamma_{20}/k_1, \gamma_{32}/k_2$, we see that the Lorentzians being acted upon by W_{KSO} may be approximated as δ functions. We make the substitution $(\gamma/\pi)/(\tilde{\Delta}^2+\gamma^2)=\delta(\Delta-kv)$, where the definition $\tilde{\Delta}=\Delta-kv$ has been used [Eqs. (7h) and (11d)]. We also specialize to $\mathbf{k}_1=k_1\hat{\mathbf{z}}$ and $\mathbf{k}_2=\epsilon k_2\hat{\mathbf{z}}$, where $\epsilon=+1$ corresponds to copropagating lasers and $\epsilon=-1$ to counterpropagating. With these approximations the line-shape expression Eq. (13) becomes

$$\rho_{33}^{\mathrm{el}}=\frac{\sqrt{\pi}}{k_1 u}e^{-(\Delta_{20}/k_1 u)^2}\frac{|V_{32}|^2|V_{20}|^2}{8\hbar^4\gamma_3\bar{\gamma}_{20}}\left[\frac{|1+\epsilon k_2/k_1|\bar{\gamma}_{20}+\bar{\gamma}_{30}}{(\Delta_{30}-[1+\epsilon k_2/k_1]\Delta_{20})^2+(|1+\epsilon k_2/k_1|\bar{\gamma}_{20}+\bar{\gamma}_{30})^2}\right.$$
$$+\frac{2\bar{\gamma}_{20}^{c}-B\bar{\Gamma}_2}{\gamma_2+B\bar{\Gamma}_2}\frac{\bar{\gamma}_{32}+(k_2/k_1)\bar{\gamma}_{20}}{(\Delta_{32}-\epsilon(k_2/k_1)\Delta_{20})^2+(\bar{\gamma}_{32}+(k_2/k_1)\bar{\gamma}_{20})^2}$$
$$\left.+\frac{2\bar{\gamma}_{20}}{\gamma_2+B\bar{\Gamma}_2}\frac{\pi}{k_2}\sum_{n=1}^{\infty}\left[\frac{B\bar{\Gamma}_2}{\gamma_2+B\bar{\Gamma}_2}\right]^n\bar{W}_K^{\,n}\left[\frac{\Delta_{20}}{k_1}\rightarrow\epsilon\frac{\Delta_{32}}{k_1}\right]\right]+(\rho_{33}^{\mathrm{el}})_{\mathrm{int}}\,, \tag{23a}$$

$$\bar{W}_K^{\,n}\left[\frac{\Delta_{20}}{k_1}\rightarrow\epsilon\frac{\Delta_{32}}{k_1}\right]=\int\cdots\int\bar{W}_K\left[v_z'\rightarrow\epsilon\frac{\Delta_{32}}{k_1}\right]\bar{W}_K(v_z''\rightarrow v_z')\cdots\bar{W}_K\left[\frac{\Delta_{20}}{k_1}\rightarrow v_z^{(n-1)}\right]dv_z^{(n-1)}\cdots dv_z''dv_z'\,. \tag{23b}$$

In this expression the superscript $(n-1)$ represents $n-1$ primes. The first Lorentzian of Eq. (23a) is the component which appears in discussions of two-photon Doppler-free line shapes and its width depends on whether the lasers are copropagating ($\epsilon=+1$) or counterpropagating ($\epsilon=-1$). For counterpropagating lasers an atom whose velocity causes one laser to appear red shifted will cause the other to appear blue shifted. Consequently when $k_1=k_2$ the sum of the photon energies is unchanged (to first order in the Doppler effect) and is equal to E_3-E_0 for any velocity. The result is that the Lorentzian width is just $\bar{\gamma}_{30}$. In the case of Na with no perturbers this amounts to a FWHM of 3 MHz (compared to a typical full Doppler width of around 1800 MHz). When the lasers are copropagating both are either red or blue shifted as viewed by an atom and so the Doppler effect is no longer suppressed for the coherent two-photon transition. In this case the FWHM is $2\bar{\gamma}_{20}+\bar{\gamma}_{30}$ when $k_1=k_2$ ($\sim$23 MHz for Na). The incoherent term is due to excitation which has been disrupted by phase-changing collisions with no velocity change. The line shape in this case is due to a convolution of Lorentzians for the $0\rightarrow2$ and $2\rightarrow3$ transitions giving rise to a linewidth of $\bar{\gamma}_{32}+\bar{\gamma}_{20}$ (for $k_1=k_2$). The positions of the Lorentzians are separated by $\bar{\delta}_{30}-\bar{\delta}_{32}-\bar{\delta}_{20}$ and so at zero pressure are coincident.

If $k_2\neq k_1$ the counterpropagating linewidths are altered due to incomplete suppression of the Doppler effect. Copropagating linewidths are also affected. For Na, $k_1/k_2=1.035$ and both the co- and counterpropagating linewidths are affected by less than 10%.

The velocity-changing part of the ρ_{33}^{el} line-shape function [Eq. (23)] in this limit has become a sum over products of the large-Δv_z part of the collision kernel. At very low perturber pressures ($\Gamma_1<\gamma_2$) where only the lowest-order (single collision) term need be kept, this contribution is simply proportional to $W_{\mathrm{KSO}}(\Delta_{20}/k_1\rightarrow\Delta_{32}/k_2)$. This is the intuitively expected result, that the experiment detects the VC kernel from an initial v in resonance with ω_1, to a final v in resonance with ω_2.

C. $\Delta_{20}\gg k_1 u$

In the limit that $\Delta_{20}\gg k_1 u$ (ω_1 tuned outside the Doppler core) two resonances occur in Eq. (13). For $\Delta_{30}\cong0$ only the two-photon, coherent term of the line-shape expression [Eq. (13)] is of importance, leading to

$$\rho_{33}^{\mathrm{el}}\cong\frac{|V_{32}|^2|V_{20}|^2}{8\hbar^4\gamma_3}\frac{1}{(\omega_1-\Omega_{20})^2}\int\frac{\gamma_{30}}{[\omega_1+\omega_2-\Omega_{30}-\bar{\delta}_{30}-(\mathbf{k}_1+\mathbf{k}_2)\cdot\mathbf{v}]^2+\bar{\gamma}_{30}^{\,2}}\rho_{00}(\mathbf{v})d^3v\,. \tag{24}$$

This is the line-shape component which arises in discussions of "two-photon" line shapes. If $k_1\neq k_2$, then the result is a Voigt profile with Gaussian width $|k_1+\epsilon k_2|u$ (in the limit that $\gamma_{30}\ll|k_1+\epsilon k_2|u$). If $k_1=k_2$ and $\epsilon=-1$ (counterpropagating) the line shape is a totally Doppler-free Lorentzian of width γ_{30}. The usual method for two-photon Doppler-free spectroscopy is to use counterpropagating beams from a single laser. Biraben *et al.*[16] have made measurements of the broadening rate $d\gamma_{30}/dP$ by this method for Na perturbed by various noble gases. Note that this broadening rate is a thermally averaged one since all velocity groups contribute equally to the line shape.

The second resonance for $\Delta_{20}\gg k_1 u$ occurs at $\Delta_{32}\cong0$, and is due to dephasing collisions. In this limit the line-shape expression becomes

$$\rho_{33}^{\rm el}\simeq\frac{|V_{32}|^2|V_{20}|^2}{8\hbar^4\gamma_3}\frac{1}{(\Omega_{20}-\omega_1)^2}\int\frac{\overline{\gamma}_{32}}{\Delta_{32}^2+\overline{\gamma}_{32}^{\,2}}\left[\frac{2\overline{\gamma}_{20}^{\,c}-\overline{\Gamma}_2}{\overline{\gamma}_{22}+\overline{\Gamma}_2}+\frac{2\overline{\gamma}_{20}}{\gamma_2+\overline{\Gamma}_2}F'_{22}(\rho_{00})\right]d^3v\ . \tag{25}$$

Since the collisional velocity redistribution cannot alter a thermal equilibrium distribution (Maxwellian) we must have

$$U_{ij}\rho_{00}=\frac{\overline{\Gamma}_{ij}}{\gamma_2+\overline{\Gamma}_2}\rho_{00}\ . \tag{26}$$

Using this expression, we can easily sum the collision series in F'_{22} to produce the following "stepwise" line shape:

$$\begin{aligned}\rho_{33}^{\rm el}&=\frac{|V_{32}|^2|V_{20}|^2}{8\hbar^4\gamma_3}\frac{1}{(\omega_1-\Omega_{30})^2}\left[\frac{2\overline{\gamma}_{20}}{\gamma_{2\,\rm eff}}-1\right]\\&\quad\times\int\frac{\overline{\gamma}_{32}}{\Delta_{32}^2+\overline{\gamma}_{32}^{\,2}}\rho_{00}(v_z)dv_z\ ,\\ \overline{\gamma}_{2\,\rm eff}&=\gamma_2\left[\frac{\gamma_2+\overline{\Gamma}_{21}+\overline{\Gamma}_{12}}{\gamma_2+\overline{\Gamma}_{21}}\right]\ .\end{aligned} \tag{27}$$

This expression has also been obtained by Liao *et al.*[9] from simple rate equation arguments. With ω_1 fixed this is a Voigt profile in ω_2. This line shape is due to atoms which have been excited to state 2 by the process $\hbar\Omega_{20}=\hbar\omega_1+\Delta E_{\rm kin}$ ($\Delta E_{\rm kin}$ is the kinetic energy change in collision) and so cannot occur without collisions. (This is called collisional redistribution in the line-broadening literature.) Depending on whether ω_1 has been tuned above or below resonance, the atomic gas will either be heated or cooled in the excitation process, an effect that has been observed experimentally by Giacombino *et al.*[17] If ω_2 is tuned to the 1-3 transition ($\Delta_{31}\cong 0$) instead of the 2-3 transition, the associated line shape is of the same form as Eq. (27). Note that γ_{32} and γ_{31} may be obtained from the widths of such "two-step" line shapes [i.e., Eq. (27) and the corresponding expression for $\Delta_{31}\cong 0$] while γ_{20} may be obtained from comparison of the relative amplitudes of the two-step and two-photon contributions[2,9] (assuming the inelastic collision rates are known).

V. NUMERICAL EVALUATION OF LINE-SHAPE EXPRESSIONS

While the approximations of Sec. IV provide insight into the components of the line-shape expressions, numerical evaluation of the full expressions is necessary to establish the validity of the approximations and to allow quantitative comparison to experiment. In Sec. V A we study the Δ_{20} ($\approx$speed) dependence of the elastic line shape [Eq. (13)] together with the behavior of its component parts. In Sec. V B we study the inelastic line shape [Eq. (14)] giving special attention to the problem of determining the kernel from an experimentally observed line shape.

A. Elastic line shape

The line-shape expression $\rho_{33}^{\rm el}(\omega_1,\omega_2)$ [Eq. (13)] contains broadening, shift, and collision rates which are functions of **v**. In a vapor where only active atom-perturber collisions are important and the perturber distribution is thermal, these rates should depend only on the speed $|\mathbf{v}|$ of the active atom. Using the results of Ward, Cooper, and Smith[12] we adopt a speed dependence based on a C_6 potential

$$\gamma(v)=\gamma_{\rm th}(1+\lambda)^{-3/10}(1+\tfrac{1}{5}\lambda x_0^2-\tfrac{7}{250}\lambda^2x_0^4+\cdots)\ ,\quad x_0\le 1 \tag{28a}$$

$$\gamma(v)=\gamma_{\rm th}\sqrt{\pi}\frac{(1+\lambda)^{-3/10}(\lambda x_0^2)^{3/10}}{2\Gamma(\frac{9}{5})}\times\left[1+\frac{6}{25\lambda x_0^2}+\frac{21}{1250\lambda^2x_0^4}+\cdots\right],\quad x_0>1\ . \tag{28b}$$

Here $\lambda=m_p/m$, $x_0=v/u$, u equals the most probable radiator speed, and $\Gamma(\frac{9}{5})$ is the gamma function. The shifts $\delta_{ij}(|v|)$ are treated as having the same speed dependence. The term $\gamma_{\rm th}$ [as well as a term $\delta_{\rm th}$ in a corresponding expression for $\delta(|v|)$] is the thermally averaged broadening (shift) which is measured in pressure broadening of Doppler line shapes. This model for the speed dependence will be used in all except the VC line-shape components where averaged rates (as discussed in Sec. IV) are used instead. By inserting Eq. (28) into the line-shape expression of Eq. (13) and using spherical coordinates, the angular part of the integrals (omitting the VC part) may be evaluated analytically. The remaining radial integrals are evaluated numerically.

In Fig. 4 are shown a series of calculated line shapes with $\Gamma_2=0$ (no state-changing or velocity-changing collisions) and $\Delta_{20}=0$ for Na with 0.0, 0.5, and 1.0 Torr Ar for both co- and counterpropagating lasers. The coherent, incoherent, and interference components are shown for each line shape. Broadening rates and shifts were taken from the review by Allard and Kielkopf[6] and were adjusted slightly using a $T^{0.3}$ dependence to correspond to the experimental temperature of Ref. 1 (495 K). The values used were $2d(\gamma_{20}/2\pi)dP=18$ MHz/Torr, $2d(\gamma_{32}/2\pi)/dP=50$ MHz/Torr, $2d(\gamma_{30}/2\pi)/dP=57$ MHz/Torr, $d(\delta_{20}/2\pi)/dP=-4.4$ MHz/Torr, $d(\delta_{32}/2\pi)/dP=-15$ MHz/Torr, and $d(\delta_{30}/2\pi)/dP=-17$ MHz/Torr at 495 K. (Recall that the γ_{ij} correspond to half widths, thus the factors of 2.) From the approximate line-shape expression of Eq. (23) we expect the ratio of the areas of the incoherent to coherent components to vary as $2\gamma_{20}^c/\gamma_2$ (for $\Gamma_2=0$). For the broadening rates used here this ratio is equal to ~ 0.9 at 0.5 Torr. It can be seen in Fig. 4 for the copropagating 0.5-Torr case that

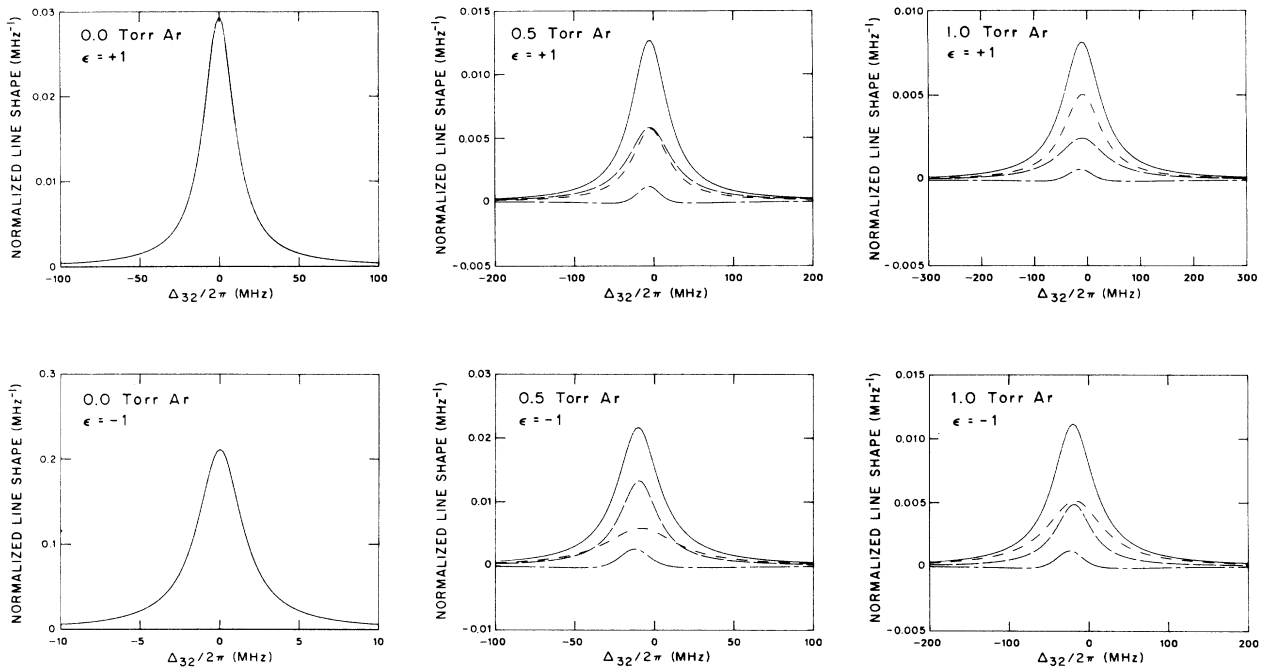

FIG. 4. Complete line shapes, ——; coherent components; — — —; incoherent components, - - -; and interference components, —·—, for co- ($\epsilon=+1$) and counterpropagating ($\epsilon=-1$) line shapes for a range of Ar perturber pressures and no VC collisions.

the coherent and incoherent components have comparable areas (as well as widths and heights) in agreement with this expectation. For the counterpropagating case the coherent term is narrower and thus has a higher peak, although the areas are still comparable. At higher pressures the incoherent term dominates while at lower pressures the coherent (two photon) term dominates. The size of the interference term depends on the differences between the broadening and shift rates [Eq. (13)], and in this case the width is intermediate to that of the coherent and incoherent terms while its peak height contributes about 10% to the total. Note that the zeros of the interference term occur approximately at the half heights of the other components, for this reason the interference term has a larger effect on the overall linewidth than might be expected when considering only its small size.

The centers of the various line-shape components have the pressure-dependent positions and intercomponent spacings expected from Sec. IV. At pressures high enough so that the linewidths are dominated by pressure broadening, the ratio of widths to intercomponent spacing is a constant and so does not further contribute to changes in the overall line shape.

Figure 5 shows a line shape for $\Delta_{20}/2\pi=-2.8$ GHz, counterpropagating lasers, and 0.25 Torr Ar ($\Gamma_2=0$). This demonstrates the transition from the limiting case of Eq. (23) ($\Delta_{20}\ll k_1 u$) to the case of Eq. (24) ($\Delta_{20}\gg k_1 u$). In the latter case the ω_1 laser is tuned far outside the Doppler width and excitation is dominated by the large number of atoms throughout the Maxwellian distribution which have been excited in their Lorentzian wings, while for $\Delta_{20}\ll k_1 u$ (ω_1 tuned inside the Doppler width) excitation is dominated by atoms which have a large enough v_z to be excited at their line center. Due to the Doppler

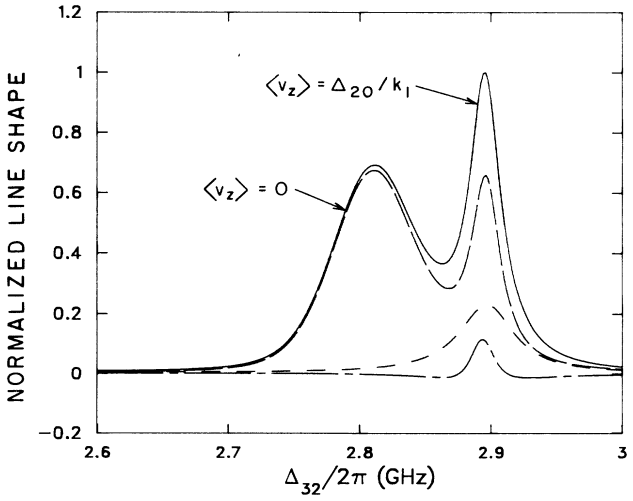

FIG. 5. Counterpropagating line shape for $\Delta_{20}/2\pi=-2.8$ GHz and 0.25 Torr Ar without VC collisions. Two distinct line shapes corresponding to the limiting cases of $\Delta_{20}\gg k_1 u$ ($\langle v_z\rangle=0$) and $\Delta_{20}\ll k_1 u$ ($\langle v_z\rangle=\Delta_{20}/k_1$) are apparent. Complete line shape, ——; coherent component, — — —; incoherent component, - - -; and interference component, —·—.

effect together with the fact that $k_1 \neq k_2$ for Na, the two limiting cases occur at different detunings. Since the population of atoms responsible for the $\Delta_{20} \gg k_1 u$ line shape have $\langle v_z \rangle = 0$, the average Doppler shift of atoms in this distribution is also zero. Consequently resonance occurs for $\Delta_{32} = -\Delta_{20}$ (neglecting collision-induced frequency shifts). The population of atoms responsible for the $\Delta_{20} \ll k_1 u$ line shape, however, has $\langle v_z \rangle = \Delta_{20}/k_1$. For this velocity group resonance will occur at $\Delta_{32}/k_2 = -\Delta_{20}/k_1$, or equivalently $\Delta_{32} = -\Delta_{20}(\lambda_1/\lambda_2)$. For Na at a detuning of $\Delta_{20} = -2.8$ GHz resonance for the small detuning line shape occurs at $\Delta_{32} = 2.8$ GHz (589nm/569 nm) = 2.9 GHz while resonance for the large detuning line shape occurs at 2.8 GHz. This accounts for the approximately 100-MHz spacing of the line shapes seen in Fig. 5. Additional shifts of both line shapes are due to collisional effects.

In Ref. 1 experimental line shapes are fit with Lorentzians in order to obtain parameters such as the linewidth. This procedure is meaningful only if the actual line shapes are very nearly Lorentzian. To test the validity of the procedure a Lorentzian has been least-squares fitted to a calculated line shape (with peak height normalized to 1) in order to see how they differ (Fig. 6). This line shape is calculated for Na perturbed by 1 Torr Ar with $\Delta_{20} = 0$ and $\Gamma_2 = 0$ (no VC collisions). Since the calculated line shape and the fitted Lorentzian agree so well, the function $E = (1-S)/(S\Delta^2)$ has been plotted in the same figure in order to emphasize the differences. If the calculated line shape (with height normalized to 1) were exactly Lorentzian $[S = (1+\Delta^2)^{-1}]$, then the function E would be exactly 1 for all Δ. Deviations from $E = 1$ represent Δ-dependent deviations from Lorentzian form. The asymmetry in $E(\Delta)$ is due to the various line-shape components having different center positions. It is apparent that the procedure of fitting a simple Lorentzian to experimental line shapes, rather than using the full line-shape expression of Eq. (13), should produce a good measurement of the line position and width.

As already noted, as Δ_{20} increases so does the v_z component of the Doppler-selected excited-state atoms. The broadening and shift must also increase with Δ_{20} since the average active atom-perturber collision rate increases as well. This effect has been studied by calculating line shapes for a range of Δ_{20} and pressures, then measuring their FWHM. The same approximations and rates as used in calculating the line shapes of Fig. 4 were used here as well with the exception that we no longer require $\Gamma_2 = 0$, i.e., VC collisions are now included. Since to a very good approximation the linewidths vary linearly with pressure in the range of interest we choose to plot the broadening rates $k_{\mathrm{Br}} = [\gamma(P, \Delta_{20})/2\pi - \gamma(P = 0, \Delta_{20})/2\pi]/P$ rather than the actual widths.

In Sec. IV we defined an effective collision temperature T_{eff} which varies as $a\Delta_{20}^2 + b$ [see Eq. (20)] with the expectation that the broadening rates would vary approximately as $T_{\mathrm{eff}}^{0.3}$. In order to test this approximation three curves of k_{Br} versus Δ_{20}^2 have been calculated for perturber-emitter mass ratios of 0.0, 1.74, and 10 000.0 (at $T = 495$ K) with $\Gamma_2 = 0$. As the ratio approaches 0.0 the perturber velocity distribution becomes much broader than that of the emitter; consequently, the collision rate for all emitters is effectively the same regardless of the emitter's velocity. For this reason the curve of k_{Br} versus Δ_{20}^2 in Fig. 7 for this case is simply a horizontal line (no Δ_{20}^2 dependence). In the case of $m_p/m = 10\,000$ the perturbers are effectively stationary resulting in the strongest possible dependence of the broadening rate on the emitters v_z. The case of $m_p/m = 1.74$ corresponds to Na perturbed by Ar. Note that all three

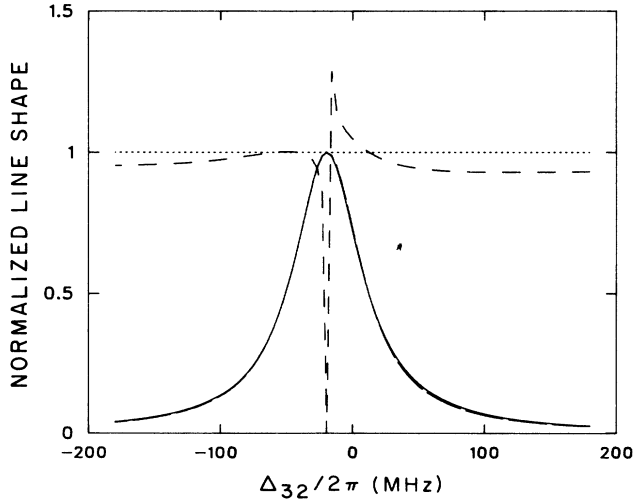

FIG. 6. Comparison of a computed line shape, ——, to a Lorentzian, — — —, for $\Delta_{20} = 0$. The function $E(\Delta_{32})$, — — —, is a sensitive measure of the difference between the calculated line shape and the Lorentzian (see text).

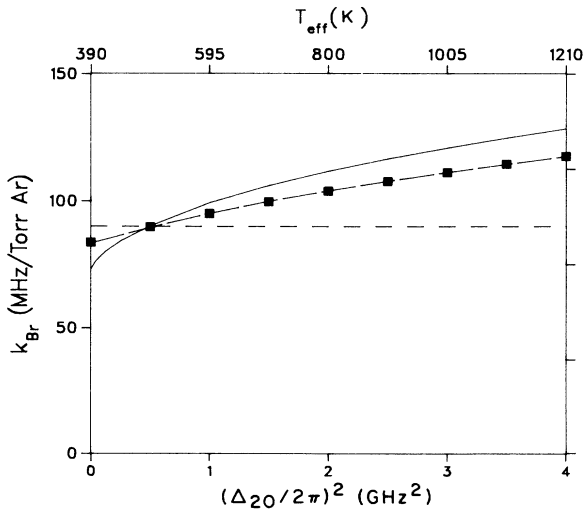

FIG. 7. Calculated broadening rates, from Eq. (13), for $m_p/m = 0$, ---; $m_p/m = 1.74$ (Ar), — — —; and $m_p/m = 10\,000$, ——. The $m_p/m = 1.74$ curve is compared to a fit with a $T_{\mathrm{eff}}^{0.3}$ dependence, ■.

curves cross at $(\Delta_{20}/2\pi)^2 \approx 0.5$ GHz^2. For the emitter vapor temperature of 495 K used here this corresponds quite well to the detuning of $(\Delta_{20}/2\pi)^2 = 0.508$ GHz^2, where $T_{\text{eff}} = T$ (independent of m_p/m). Since velocity-dependent terms enter Eq. (13) in many ways, $v^{3/5}$-dependent γ_{ij}^c need not lead to an overall $T_{\text{eff}}^{0.3}$ dependence for k_{Br}. To test $k_{\text{Br}} \propto T_{\text{eff}}^{0.3}$ ($\propto a\Delta_{20}^2 + b$) the curve corresponding to $m_p/m = 1.74$ was fit to a function of this form. The solid squares of Fig. 7 are a plot of this function. As can be seen, the k_{Br} calculated from the full expression does follow a $T_{\text{eff}}^{0.3}$ dependence very accurately.

In Fig. 8 the broadening rates (due to Ar) of the coherent and incoherent line-shape components as well as of complete line shapes are plotted versus Δ_{20}^2 and T_{eff} for several values of Γ_2 (VC collision rates). The corresponding experimental data from Ref. 1 have also been plotted. Here we have assumed that all VC collisions produce a Δv_z large enough that these atoms are removed from the line core. In this limit we may neglect the VC part of the line-shape expression [last term in the integrand of Eq. (13)] when studying the component linewidths and broadening rates. The broadening rate of the complete line shape will be in a range bounded approximately by the largest and smallest rates of the component parts. It is also affected by the change in relative importance of the component parts with v_z. Part (a) of Fig. 8 deals with line shapes produced using copropagating ($\epsilon = +1$) lasers. In this case the coherent component has the largest broadening rate and the incoherent component the smallest. The broadening rate of the interference term (not shown in the figure) is intermediate to these two. Because no values for Γ_2 (the total VC rate) are available, curves for broadening rates of the full line shape are shown for velocity-changing collision rates of (at 1 Torr Ar) $\Gamma_2 = 0$, $2\gamma_{20}^c/2$ (=9 MHz), and $2\gamma_{20}^c$ (=18 MHz). From Eq. (13) it can be seen that increasing Γ_2 has the effect of decreasing the incoherent contribution to the line core. At $\Gamma_2 = 2\gamma_{20}^c$ the incoherent component is com-

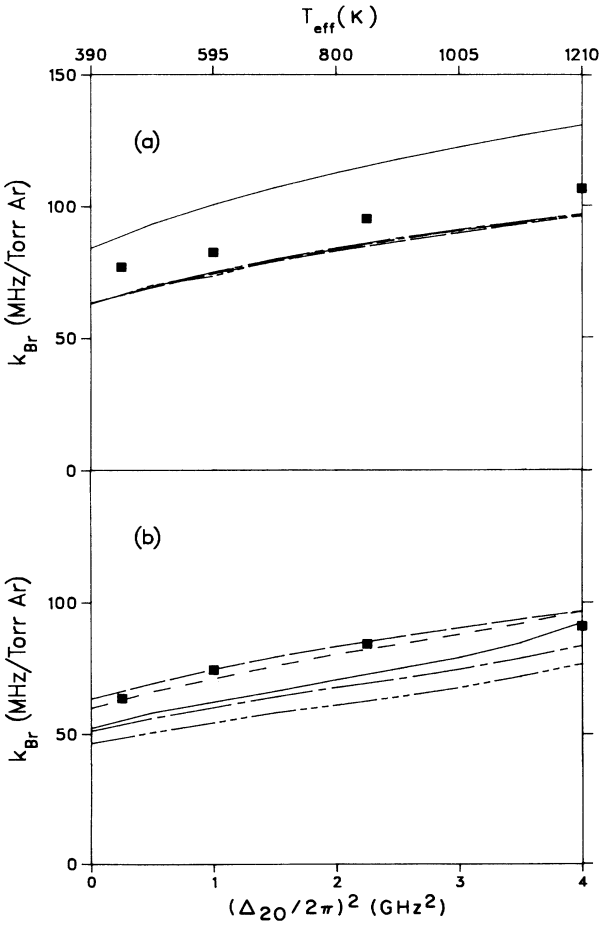

FIG. 8. Broadening rates for coherent terms, ——; incoherent terms, — — —; and complete line shapes with $\Gamma_2 = 0$, - - -; $\Gamma_2 = 2\gamma_{20}^c/2$, — - —; and $\Gamma_2 = 2\gamma_{20}^c$, ——- —— with Ar perturbers. Part (a) is for copropagating lasers and (b) for counterpropagating lasers. The ■ are experimental rates from Ref. 1.

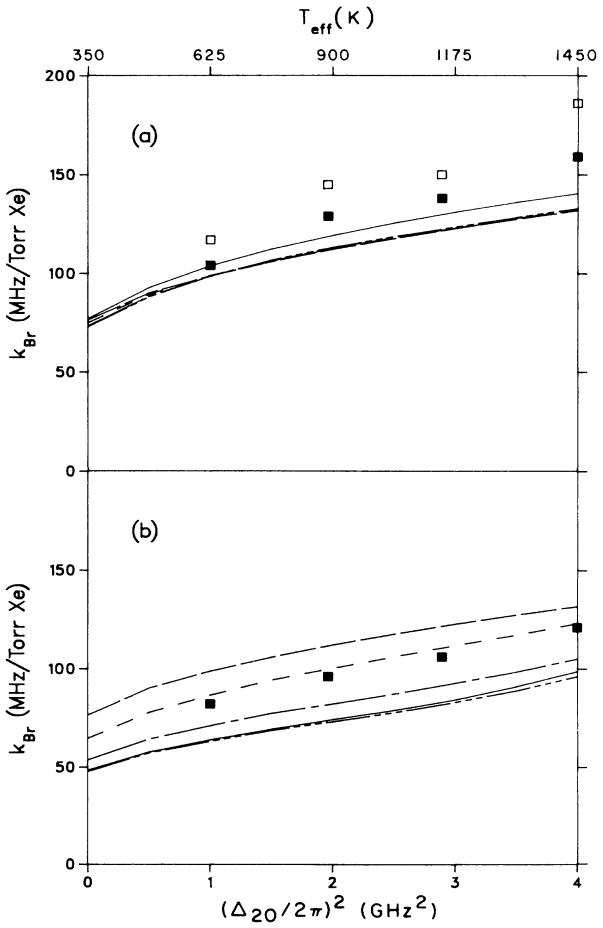

FIG. 9. Broadening rates for coherent terms, ——; incoherent terms, — — —; and complete line shapes with $\Gamma_2 = 0$, - - -; $\Gamma_2 = 2\gamma_{20}^c/2$, — - —; and $\Gamma_2 = 2\gamma_{20}^c$, ——- ——, with Xe perturbers. Part (a) is for copropagating lasers and (b) for counterpropagating lasers.

pletely eliminated. In this limit the line core is determined entirely by the coherent and interference components. In the specific case of Na-Ar broadening rates used here, the combination of the coherent and interference terms produces broadening comparable to that of the incoherent term. Consequently, varying Γ_2 has very little effect on the broadening of the complete line shape, as demonstrated by the overlapping curves of Fig. 8(a). Also shown in Fig. 8(a) are data points from the experiment of Ref. 1. While the data seem to follow the same T_{eff} dependence of the calculations, the values differ by about 10%.

The calculations of Fig. 8(a) have been repeated in Fig. 8(b) for the case of counterpropagating lasers ($\epsilon=-1$). Here it is seen that the broadening of the complete line shape can actually be less than that of either the coherent or incoherent term. This is due to effect of the interference term which adds to the line shape at the center and subtracts in the wings, thus narrowing the complete line shape. It is also apparent here that varying Γ_2 from 0 to $2\gamma_{20}^c$ causes the broadening rate of the complete line shape to drop by about 20%. Unlike the copropagating linewidth, the counterpropagating linewidth is quite sensitive to the VC collision rate Γ_2. The agreement between calculation and data is best for $\Gamma_2=0$ and worst for $\Gamma_2=2\gamma_{20}^c$.

Figure 9 is the same as Fig. 8 but for Xe perturbers rather than Ar. The behavior of both theory and data is qualitatively similar to that for Ar perturbers. Broadening rates and shifts for Na perturbed by Xe were also taken from the review by Allard and Kielkopf[6] and were adjusted in the same way as described for the Ar perturber rates. The values used were $2d(\gamma_{20}/2\pi)/dP=18$ MHz/Torr, $2d(\gamma_{32}/2\pi)/dP=69$ MHz/Torr, $2d(\gamma_{30}/2\pi)/dP=57$ MHz/Torr, $d(\delta_{20}/2\pi)/dP=-3.4$ MHz/Torr, $d(\delta_{32}/2\pi)/dP=-21$ MHz/Torr, and $d(\delta_{30}/2\pi)/dP=-18$ MHz/Torr. (Recall that the γ_{ij} correspond to half widths.)

The discrepancy (around 10%) between the theoretical curves and data in Figs. 8 and 9 is comparable to the uncertainty in the measured thermally averaged broadening rates used for the calculations. Another possible source for this discrepancy is in the approximation that all VC collisions produce a large Δv_z. If there were a significant number of small-Δv_z collisions they could play an important role in determining the linewidth. To explore this possibility the line-broadening calculations were repeated using the kernel of Eq. (17) which consists of a narrow Lorentzian component plus a broad Keilson-Storer component. To simplify computations the Keilson-Storer part of the kernel was omitted. This omitted component is about two orders of magnitude broader than the line core under consideration, so it contributes only a negligibly small baseline to the central line shape. We must also choose a value for the velocity-changing (elastic plus inelastic) rate Γ_2. An estimate of this rate may be obtained by assuming a C_6 interaction potential whose scattering cross section is given by the Landau-Lifshitz-Schiff approximation[18] $\sigma_{\text{LLS}}=8.083\ (C/v)^{2/5}$ (a.u.). For the Na($3P$)-Ar interaction the constant C is[19] 461 (a.u.). Using the average interatomic collision velocity for v (at 495 K) the estimated collision rate is[20] (in frequency units) 16 MHz/Torr. While this number cannot be correct in detail due to the obvious neglect of inelastic collisions (the potential must be more complex than C_6) it nevertheless indicates that Γ_2 is probably comparable to $2\bar{\gamma}_{20}^c$, which is 18 MHz for Na perturbed by 1 Torr Ar. We therefore make the approximation that all collisions are velocity changing, i.e., $\Gamma_2=2\gamma_{20}^c$. In this limit the incoherent term, which represents dephasing without VC, vanishes and is replaced by the VC component. This seems intuitively plausible and maximizes the importance of the collision kernel. Finally, in order to simplify the integrals in the VC part of Eq. (13) the speed-dependent broadenings and shifts are replaced by averaged values using the $\bar{\gamma},\bar{\delta}\propto T_{\text{eff}}^{0.3}$ approximation. Based on known inelastic cross sections[21] for Na perturbed by Ar the inelastic collision rates are[20] $\Gamma_{21}=1.5$ MHz, $\Gamma_{12}=3$ MHz (1 Torr Ar). Since $\Gamma_{12},\Gamma_{21}\ll\Gamma_2$ we will for simplicity set $\Gamma_{12},\Gamma_{21}=0$ (no inelastic collisions) when calculating the elastic line shapes. Note that with a Lorentzian kernel all of the collision integrals of Eq. (16b) are successive convolutions of Lorentzians which in turn produce Lorentzians. The VC part of the line shape in this case becomes, in terms of the width w of the Lorentzian component of the kernel [Eq. (17)],

$$(\rho_{33}^{\text{el}})_{\text{VC}}(\omega_1,\omega_2)=\frac{|V_{32}|^2|V_{20}|^2}{4\hbar^4\gamma_3}\frac{\sqrt{\pi\ln 2}}{\Omega_D}e^{-\ln 2(\Delta_{20}/\Omega_D)^2}\frac{1}{\gamma_2+\bar{\Gamma}_2}$$
$$\times\sum_{n=1}^{\infty}\left[\left[\frac{A\bar{\Gamma}_{22}}{\bar{\Gamma}_{22}+\gamma_2}\right]^n\frac{\left[\bar{\gamma}_{32}+\frac{k_2}{k_1}(\bar{\gamma}_{20}+nk_1w)\right]}{\left[\Delta_{32}-\epsilon\frac{k_2}{k_1}\Delta_{20}\right]^2+\left[\bar{\gamma}_{32}+\frac{k_2}{k_1}(\bar{\gamma}_{20}+nk_1w)\right]^2}\right]. \tag{29}$$

In computing the line shape using the kernel of Eq. (17) the parameters w and A must be specified. Various values for these parameters were tried and it was found that the data for Ar perturbers are best fit using a Lorentzian width (FWHM) of about 6 MHz ($k_1w/2\pi=\frac{6}{2}=3$ MHz) with the Lorentzian accounting for 95% of the kernel ($A=0.95$). For Xe the width was found to be 35 MHz with the Lorentzian accounting for

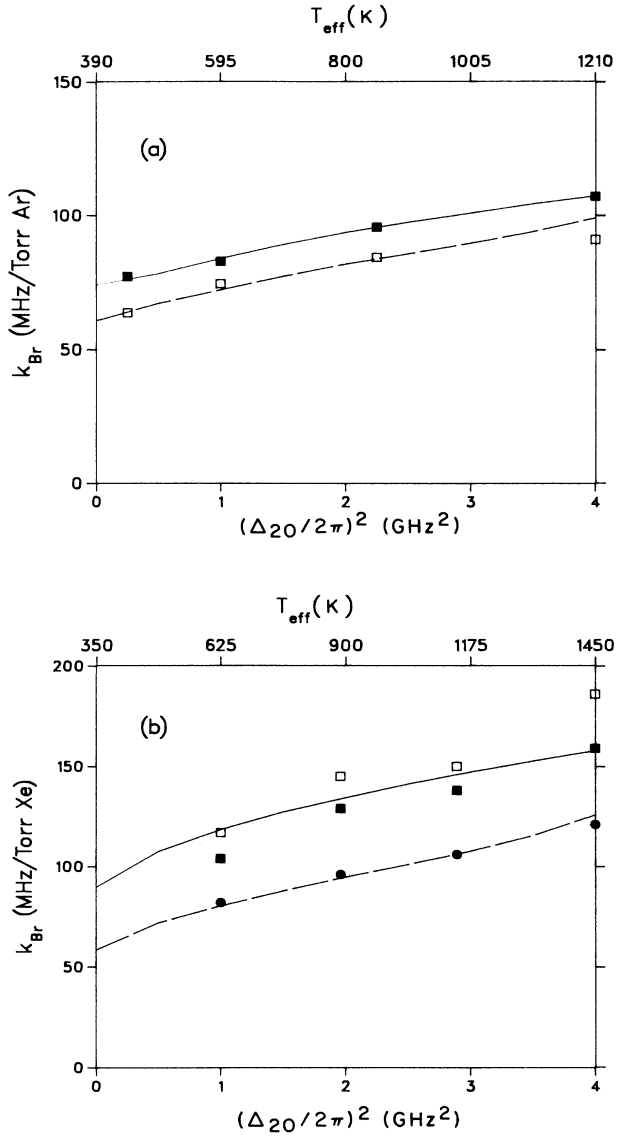

FIG. 10. Comparison of experimental broadening data to best-fit calculations. All theoretical curves use $\Gamma_2=2\gamma^c_{20}$. (a) $3S$-$3P_{1/2}$-$4D$ broadened by Ar: ■, measured values with $\epsilon=+1$; □, measured values with $\epsilon=-1$; ——, calculated curve for $\epsilon=+1$; ---, calculated curve for $\epsilon=-1$. (b) $3S$-$3P_{1/2}$-$4D$ broadened by Xe: □, measured $3S$-$3P_{1/2}(F=2)$-$4D_{3/2}$ rates for $\epsilon=+1$; ■, measured $3S$-$3P_{1/2}(F=1)$-$4D_{3/2}$ rates for $\epsilon=+1$; ●, measured $3S$-$3P_{1/2}$-$4D$ rates for $\epsilon=-1$; ——, calculated curve for $\epsilon=+1$; ---; calculated curve for $\epsilon=-1$.

75% of the kernel. Broadening rates versus Δ^2_{20} for both Ar and Xe perturbers have been plotted together with experimental data[1] in Fig. 10. The w and A parameters had to be chosen such that good agreement between theory and data was obtained for both co- and counterpropagating broadening rates. Table I contains broadening rates calculated at $(\Delta_{20}/2\pi)^2=2$ GHz^2 for a few values of Lorentzian kernel widths w and fractional contributions

TABLE I. Co- and counterpropagating broadening rates for Na-Ar at a few values of A and w. A is the fraction of the kernel accounted for by a Lorentzian and $2w$ is its width. For these calculations $\Delta^2_{20}=2$ GHz^2 and $\Gamma=2\gamma^c_{20}$.

		k_{Br} (MHz/Torr)	
A	$2k_1w/2\pi$ (MHz)	$\epsilon=+1$	$\epsilon=-1$
0.9	5	114.4	82.26
0.9	10	119.5	83.44
1.0	5	116.4	86.88
1.0	10	123.1	88.65

A in order to demonstrate the degree of sensitivity of the calculated broadening rates to these parameters. The values of the kernel parameters obtained by this analysis are also functions of the elastic (Γ_{22}) and inelastic (Γ_{21}) collision rates.

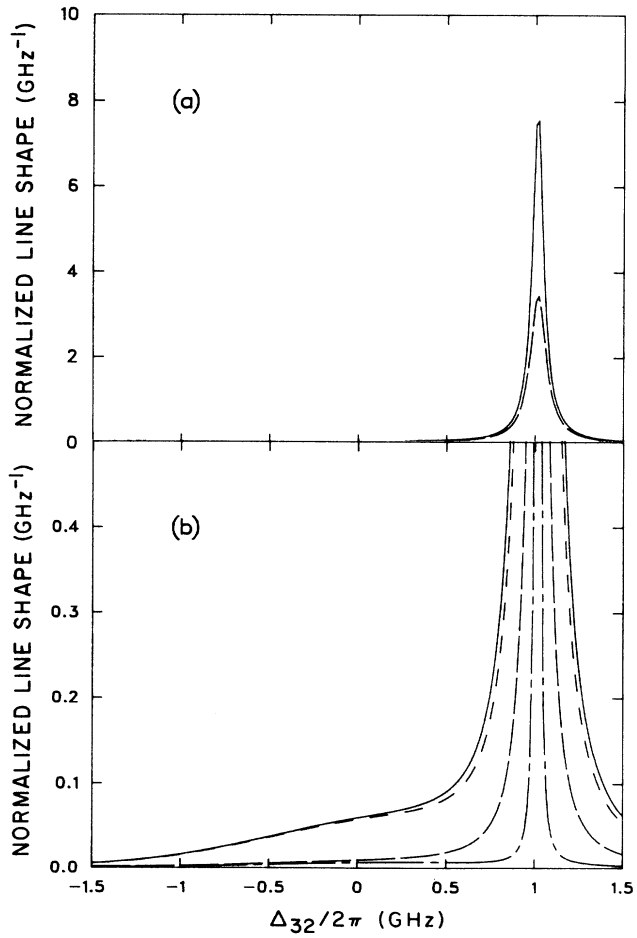

FIG. 11. Calculated Na elastic line shape ρ^{el} for $\Delta_{20}/2\pi=-1$ GHz, 1 Torr Ar, and counterpropagating lasers. The area of the line shape has been normalized to 1. (a) complete line shape, ——; VC contribution, ———. (b) complete line shape, ——; VC contribution, — — —; single VC collision contribution, - - -; elastic kernel, —·—.

The central core of Ho and Chu's kernel[15] for Na($3S$)-Ar collisions (calculated at 300 K) varies in width from 9 MHz for $v_z=0$ to about 3 MHz for $v_z=2u$. As shown in Sec. III the Lorentzian accounts for about 92% of the entire kernel for $v_z=0$. The width of the kernel decreases with increasing relative speed because at higher speeds the collisional interaction time is shorter, thus less momentum is exchanged for the same interatomic force and impact parameter. Extrapolating from the calculations of Ho and Chu we estimate the kernel width would vary from approximately 6 to 1.6 MHz as v_z varies from 0 to $2u$ at the temperature of 495 K used in the calculations presented here. The narrower kernel is due to the larger interatomic speeds at the higher temperature. Thus, kernel parameters that were found to best match the experimental Ar broadening rates are consistent with those inferred from Ho and Chu's calculations. It must be kept in mind, however, that the experimental kernel was for Na($3P$)-Ar collisions whereas Ho and Chu's calculation was for Na($3S$)-Ar collisions. Furthermore, we have not allowed for a speed-dependent kernel width in the computations.

To study the complete line shape including the effect of large-Δv collisions the entire kernel of Eq. (17) is used. Again the speed-dependent rates are replaced with their averaged values. Using the expression of Eq. (16) for the velocity-changing part of the line shape together with the expression for F'_{22} obtained in the Appendix, the velocity-changing contribution to the line shape in this approximation is obtained

$$[\rho_{33}^{\mathrm{el}}(\omega_1,\omega_2)]_{\mathrm{VC}}=\frac{|V_{32}|^2|V_{20}|^2}{4\hbar^4\gamma_3}\frac{1}{\gamma_2+\bar{\Gamma}_2}\sum_{n=1}^{\infty}\left[\frac{A\bar{\Gamma}_2}{\gamma_2+\bar{\Gamma}_2}\right]^n\frac{\bar{\gamma}_{32}+\frac{k_2}{k_1}(\bar{\gamma}_{20}+nk_1w)}{\left[\Delta_{32}-\epsilon\frac{k_2}{k_1}\Delta_{20}\right]^2+\left[\bar{\gamma}_{32}+\frac{k_2}{k_1}(\gamma_{20}+nk_1w)\right]^2}$$

$$+\frac{1}{\gamma_2+B\bar{\Gamma}_2}\sum_{n=1}^{\infty}\left[\frac{B\bar{\Gamma}_2}{\gamma_2+B\bar{\Gamma}_2}\right]^n\int\frac{\bar{\gamma}_{32}}{\tilde{\Delta}_{32}^2+\bar{\gamma}_{32}^2}\left[\int\frac{\exp\left[-\left[\frac{v_z-\alpha^n v_z'}{u(1-\alpha^{2n})^{1/2}}\right]^2\right]}{\sqrt{\pi}u(1-\alpha^{2n})^{1/2}}\frac{\bar{\gamma}_{20}}{\tilde{\Delta}_{20}^2+\bar{\gamma}_{20}^2}\times\rho_{00}(v_z')dv_z'\right]dv_z\ . \tag{30}$$

In Fig. 11(a) are shown a complete line shape and the velocity-changing component for $\Delta_{20}/2\pi=-1$ GHz, counterpropagating beams ($\epsilon=-1$), and 1 Torr Ar. The collision kernel parameters used are $A=0.95$, $2k_1w/2\pi=6$ MHz, $\alpha=0.2$, and $\bar{\Gamma}_2=2\gamma_{20}^c$. In Fig. 11(b) these same curves together with the single-collision contribution and the single-collision (elastic) kernel are shown using an expanded vertical scale. The elastic kernel was obtained from the single-collision line-shape contribution by allowing the radiative linewidths to go to zero. It is apparent that starting about 100 MHz from the line core the line shape is heavily dominated by the velocity-changing contribution. Comparing the VC component to its single-collision contribution it is clear that multiple collisions account for a large part of the line shape at this pressure, thus making it difficult to infer the underlying collision kernel from an experimental line shape. The same calculation has been repeated for a pressure of 0.2 Torr Ar in Fig. 12. Though the single-collision contribution now represents a much larger fraction of the VC term, the line shape does not become dominated by the VC term until 300–400 MHz from the line core. Again it would be difficult to infer the kernel from experimental data except perhaps at very large collisional velocity changes. Figure 13 is for the same conditions as Fig. 11 except that copropagating ($\epsilon=+1$) beams are used. It is qualitatively similar to the counterpropagating line shape in the way it is affected by VC collisions.

B. Inelastic line shapes

In evaluating the inelastic line shape [Eq. (16c)] we again use the kernel of Eq. (17). In contrast to the calculation of ρ^{el} where only one type of collision (elastic VC) had to be considered, both elastic and inelastic VC effects must be included. The full inelastic collision operator

$$F'_{12}=\sum_{n=0}^{\infty}U'^{n}_{11}U'_{12}\sum_{m=0}^{\infty}\left[U'_{22}+U'_{21}\sum_{l=0}^{\infty}U'^{l}_{11}U'_{12}\right]^m$$

must be considered. First note that $U'_{21},U'_{12}\propto\Gamma_{21}/(\gamma_2+\Gamma_2)=0.07$. Here we have used $(\gamma_2/2\pi)=10$ MHz, $\Gamma_2/2\pi=(\Gamma_{21}+\Gamma_{22})/2\pi=18$ MHz, $\Gamma_{21}/2\pi=2$ MHz, and $\Gamma_{22}/2\pi=16$ MHz at 1 Torr Ar. For elastic collisions $U'_{22}\propto\Gamma_{22}/(\gamma_2+\Gamma_2)=0.6$. These rates are the same as used for the ρ^{el} line-shape calculation with the exception that now $\Gamma_2\neq\Gamma_{22}$ due to the inclusion of inelastic collisions. For simplicity we assume $\Gamma_{12}=\Gamma_{21}$, $\Gamma_{11}=\Gamma_{22}$. Within the bracket of the expression for F_{12} we see that the ratio of the $l=0$ term to U'_{22} is $U'_{21}U'_{12}/U'_{22}\cong0.01$. While a careful comparison of these terms requires looking in detail at the kernels, this simple comparison suggests that only a small error will be introduced by neglecting the inelastic collision operators within the bracket. With this simplification the full collision operator becomes

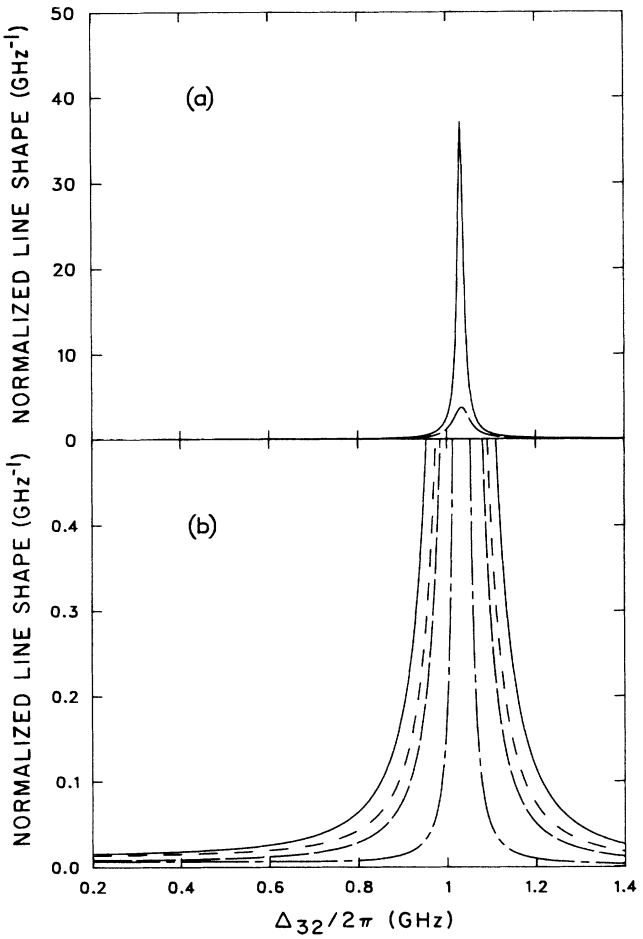

FIG. 12. Calculated Na elastic line shape ρ^{el} for $\Delta_{20}/2\pi=-1$ GHz, 0.2 Torr Ar, and counterpropagating lasers. The area of the line shape has been normalized to 1. (a) complete line shape, ——; VC contribution, — — —. (b) complete line shape, ——; VC contribution, — — —; single VC collision contribution, - - -; elastic kernel, —·—.

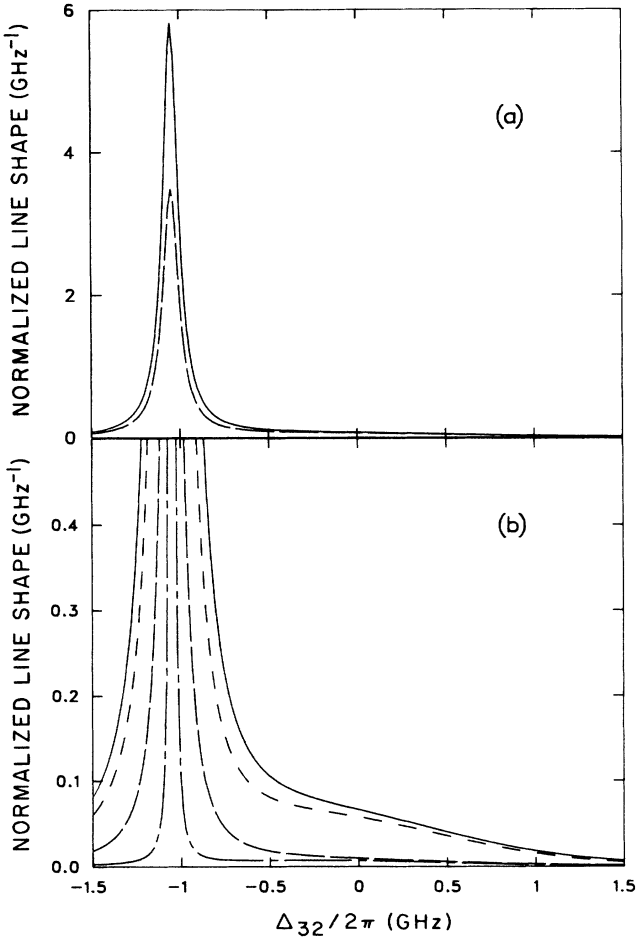

FIG. 13. Calculated Na elastic line shape ρ^{el} for $\Delta_{20}/2\pi=-1$ GHz, 1 Torr Ar, and copropagating lasers. The area of the line shape has been normalized to 1. (a) complete line shape, ——; VC contribution, — — —. (b) complete line shape, ——; VC contribution, — — —; single VC collision contribution, - - -; elastic kernel, —·—.

$$F'_{12}=\sum_{n=0}^{\infty} U'^{n}_{11}U'_{12}\sum_{m=0}^{\infty} U'^{m}_{22}\ .$$

In Sec. III we saw that the experimentally determined inelastic kernel could be fit fairly well by the kernel of Eq. (17) with the choices $2(k_1w'/2\pi)=125$ MHz, $A'=0.8$, $\alpha=0.2$. In calculating the inelastic line shape this kernel will be used for U'_{12},U'_{21}, and the kernel used for calculating the elastic line shape will again be used here for U'_{11},U'_{22}. For this elastic kernel $2(k_1w/2\pi)=6$ MHz, $A=0.95$, $\alpha=0.2$. Using the expression for $\sum_{n=1}^{\infty}U'^{n}$ obtained in the Appendix with the approximations introduced above the inelastic line-shape expression becomes

$$\rho^{in}_{33}(\omega_1,\omega_2)=\frac{|V_{31}|^2|V_{20}|^2}{4\hbar^4\gamma_3}\frac{1}{\gamma_2+\bar{\Gamma}_2}\int\frac{\bar{\gamma}_{31}}{\tilde{\Delta}^2_{31}+\bar{\gamma}^2_{31}}\sum_{n=0}^{\infty}U'^{n}_{11}U'_{12}\sum_{m=0}^{\infty}U'^{m}_{22}\left[\frac{\bar{\gamma}_{20}}{\tilde{\Delta}^2_{20}+\bar{\gamma}^2_{20}}\rho_{00}\right]dv_z$$

$$=\frac{|V_{31}|^2|V_{20}|^2}{4\hbar^4\gamma_3}\frac{1}{\gamma_2+\bar{\Gamma}_2}\int G(\Delta_{31},k_1v_z)\frac{\bar{\Gamma}_{12}}{\gamma_2+\bar{\Gamma}_2}W_{21}(k_1v'_z\rightarrow k_1v_z)H(k_1v'_z,\Delta_{20})d(k_1v'_z)d(k_1v_z)\ , \tag{31a}$$

$$G(\Delta_{31},v_z)=\sum_{n=0}^{\infty}\left[\frac{A\bar{\Gamma}_{22}}{\gamma_2+\bar{\Gamma}_2}\right]^n\frac{\bar{\gamma}_{31}+nk_2w}{\tilde{\Delta}_{31}^2+(\bar{\gamma}_{32}+nk_2w)^2}+\frac{\gamma_2+\bar{\Gamma}_2}{\gamma_2+B\bar{\Gamma}_{22}+\bar{\Gamma}_{21}}$$
$$\times\sum_{n=1}^{\infty}\left[\frac{B\bar{\Gamma}_{22}}{\gamma_2+B\bar{\Gamma}_{22}+\bar{\Gamma}_{21}}\right]^n\frac{\sqrt{\pi}\exp\left[-\left[\frac{(k_1/k_2)\Delta_{31}-\alpha^n k_1v_z}{k_1u(1-\alpha^{2n})^{1/2}}\right]^2\right]}{k_1u(1-\alpha^{2n})^{1/2}}, \tag{31b}$$

$$W_{21}(k_1v_z'\to k_1v_z)=\frac{A'}{\pi}\frac{k_1w'}{(k_1v_z-k_1v_z')^2+(k_1w')^2}+\frac{B'}{\sqrt{\pi}k_1u(1-\alpha^2)^{1/2}}\exp\left[-\left[\frac{k_1v_z-\alpha k_1v_z'}{k_1u(1-\alpha^2)^{1/2}}\right]^2\right], \tag{31c}$$

$$H(k_1v_z',\Delta_{20})=\frac{e^{-(\Delta_{20}/k_1u)^2}}{k_1u\sqrt{\pi}}\left\{\sum_{n=0}^{\infty}\left[\frac{A\bar{\Gamma}_{22}}{\gamma_2+\bar{\Gamma}_2}\right]^n\frac{\bar{\gamma}_{20}+nk_1w}{\tilde{\Delta}_{20}^2+(\bar{\gamma}_{20}+nk_1w)^2}+\frac{\gamma_2+\bar{\Gamma}_2}{\gamma_2+B\bar{\Gamma}_{22}+\bar{\Gamma}_{21}}\right.$$
$$\left.\times\sum_{n=1}^{\infty}\left[\frac{B\bar{\Gamma}_{22}}{\gamma_2+B\bar{\Gamma}_{22}+\bar{\Gamma}_{21}}\right]^n\frac{\sqrt{\pi}\exp\left[-\left[\frac{k_1v_z'-\alpha^n\Delta_{20}}{k_1u(1-\alpha^{2n})^{1/2}}\right]^2\right]}{k_1u(1-\alpha^{2n})^{1/2}}\right\}. \tag{31d}$$

Figure 14(a) shows a calculated Na inelastic line shape ρ^{in} for $\Delta_{20}/2\pi=-1$ GHz at 1 Torr Ar. Also shown is the line-shape contribution due to atoms which have undergone a single inelastic collision ($2\to1$) and no VC collisions. Clearly VC collisions before and after the inelastic collision contribute significantly to the line shape. This "single inelastic collision" contribution is just the convolution of the $0\to2$, $1\to3$ line-shape functions with the inelastic kernel. In Fig. 14(b) calculated ρ^{in} line shapes at $\Delta_{20}/2\pi=-1$ GHz are shown for 1.0, 0.67, and 0.33 Torr Ar. Also shown is the inelastic kernel. The area of each line shape and that of the kernel has been normalized to 1 for comparison. As the perturber pressure approaches zero the line shape approaches a limit in which it becomes simply the convolution of the $0\to2$, $1\to3$ Lorentzian line-shape functions with the inelastic kernel. By experimentally observing inelastic line shapes at a series of low perturber pressures the $P\to0$ limiting line shape may be determined by extrapolation. The inelastic kernel can then be obtained by deconvolving this $P\to0$ line shape using known $0\to2$, $1\to3$ natural linewidths. This is the method used in Ref. 1 to determine the inelastic kernel shown in Fig. 3. A complicating factor which we have neglected here is the existence of multiple overlapping hyperfine level line-shape components. Also, the deconvolution process is very sensitive to noise in the data. Methods for overcoming these difficulties in the line-shape analysis are presented in Ref. 1.

The ρ^{in} line shape observed in the experiment of Ref. 1 seems to have a stronger pressure dependence than shown by the calculated line shapes of Fig. 14. This could possibly be due to an underestimate of the importance of multiple inelastic collisions or of the width of the small-Δv_z part of the elastic collision kernel. An underestimate of the elastic kernel width could be due to an overestimate of the elastic velocity-changing collision rate in the line-shape calculations of Sec. V A.

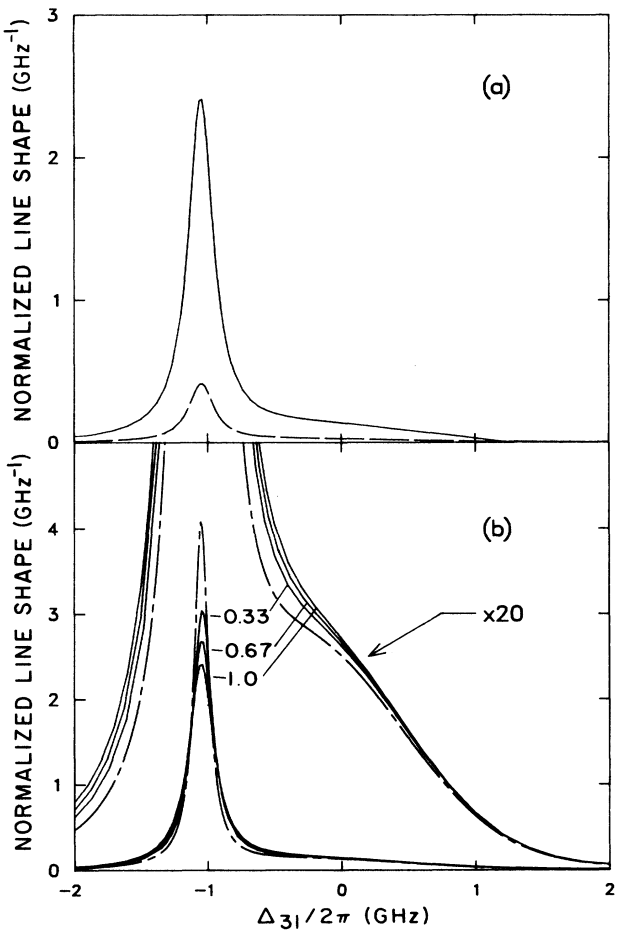

FIG. 14. Calculated Na inelastic line shape ρ^{in} for $\Delta_{20}/2\pi=-1$ GHz. (a) 1 Torr Ar: complete line shape, ——; no elastic VC contribution, — — —. (b) The three solid curves are line shapes at 1.0, 0.67, and 0.33 Torr Ar. The area of each line shape is normalized to 1. The inelastic kernel (area normalized to 1) is given by the dashed line.

VI. SUMMARY

We have derived expressions for two-photon–two-step line shapes in the presence of both elastic and inelastic

(fine-structure-changing) collisions. These expressions consist of terms clearly identifiable as coherent, incoherent, interference, and VC contributions. At low pressures (where the collision rate is less than the radiative decay rates) the line shape is dominated by the coherent term. As the perturber pressure increases the incoherent, interference, and velocity-changing terms become dominant. Line shapes for excitation via $0\rightarrow 2\rightarrow 3$ $[\rho^{\mathrm{el}}(\omega_1,\omega_2)]$ and $0\rightarrow 2\rightarrow(\text{collision})\rightarrow 1\rightarrow 3$ $[\rho^{\mathrm{in}}(\omega_1,\omega_2)]$ were derived.

As ω_1 is varied within the Doppler width of the (0-2) transition state-2 populations with different v_z are generated. Higher values of v_z have larger collision rates, broadenings, and shifts. Modeling the atomic interaction as a C_6 potential, calculations were performed showing that the broadening rate of the $\rho^{\mathrm{el}}(\omega_1,\omega_2)$ line shape varies as $T_{\mathrm{eff}}^{0.3}$. T_{eff} is an "effective" collisional temperature based on the rms collision velocity of the population of atoms having a $\hat{\mathbf{z}}$ component of velocity which brings them into resonance with ω_1.

Using a kernel similar to that calculated by Ho and Chu[15] and assuming that all collisions are velocity changing in nature ($\Gamma_2=2\gamma_{20}^c$), good agreement between calculated ω_2-dependent broadening rates of the ρ^{el} line shape and those measured by experiment[1] was found. Using a Keilson-Storer kernel alone was insufficient, a narrow component (Lorentzian) which accounts for the effect of small-Δv_z collisions had to be added to the Keilson-Storer kernel in order to explain the data. Due to the number of parameters involved and the uncertainties in the width and shift parameters γ,δ used in the computations we do not claim to have determined the kernel parameters by this method. However, we have demonstrated the role and relative importance of the various physical processes which cause line broadening. In particular, these calculations show that the simple Keilson-Storer and hard-sphere kernels alone are inadequate for explaining complete line shapes due to their neglect of small-Δv_z collisions.

As the perturber pressure increases the ρ^{el} line shape eventually becomes dominated by the state-2 velocity distribution. By this point, however, multiple collisions must be included to account for the line shape. In contrast to this the ρ^{in} line shape is dominated by the state-1 velocity distribution at all pressures. It was shown that at extremely low pressures (where the collision rate is much less than the radiative decay rate) the core of the line shape is just the convolution of Lorentzian line-shape functions with the collision kernel, and outside this (in the wings) the line shape is directly proportional to the kernel. Thus the inelastic line shape provides a unique opportunity to directly determine a collision kernel by experiment. This has been done in Ref. 1.

ACKNOWLEDGMENTS

This work was supported by the National Science Foundation under Grant No. PHY86-04504 through the University of Colorado.

APPENDIX

By using the collision kernel of Eq. (17), the collision operator F'_{22} [Eq. (16a)] becomes

$$F'_{22}=\sum_{m=1}^{\infty}\left[\frac{\overline{\Gamma}_2}{\gamma_2+\overline{\Gamma}_2}(AW_{\mathrm{LO}}+BW_{\mathrm{KSO}})\right]^m . \tag{A1}$$

Here we have assumed that no inelastic collisions occur ($U'_{12},U'_{21}=0$). The Keilson-Storer collision operator W_{KSO} has been defined in Eq. (22). The Lorentzian collision operator is

$$\begin{aligned} W_{\mathrm{LO}}\rho&=\int W_L(v_z'-v_z)\rho(v_z')dv_z' ,\\ W_L(v_z'-v_z)&=\frac{1}{\pi}\frac{w}{(v_z-v_z')^2+w^2} . \end{aligned} \tag{A2}$$

Using the binomial expansion we rewrite Eq. (A1)

$$F'_{22}=\sum_{m=0}^{\infty}\sum_{n=0}^{m}\left[\frac{A\overline{\Gamma}_2W_{\mathrm{LO}}}{\gamma_2+\overline{\Gamma}_2}\right]^{m-n}\left[\frac{B\overline{\Gamma}_2W_{\mathrm{KSO}}}{\gamma_2+\overline{\Gamma}_2}\right]^n \times\binom{m}{n}-1 . \tag{A3}$$

We now make use of the fact that the Lorentzian kernel is generally orders of magnitude narrower than the Keilson-Storer kernel. When products such as $W_{\mathrm{LO}}W_{\mathrm{KSO}}$ occur the Lorentzian may be approximated as a δ function so that $W_{\mathrm{LO}}W_{\mathrm{KSO}}=W_{\mathrm{KSO}}$. Equation (A3) may now be rewritten as

$$\begin{aligned} F'_{22}=&\sum_{m=0}^{\infty}\left[\frac{A\overline{\Gamma}_2W_{\mathrm{LO}}}{\gamma_2+\overline{\Gamma}_2}\right]^m\binom{m}{0}-\sum_{m=0}^{\infty}\left[\frac{A\overline{\Gamma}_2}{\gamma_2+\overline{\Gamma}_2}\right]^m\binom{m}{0}\\ &+\sum_{m=0}^{\infty}\sum_{n=0}^{m}\left[\frac{A\overline{\Gamma}_2}{\gamma_2+\overline{\Gamma}_2}\right]^{m-n}\left[\frac{B\overline{\Gamma}_2W_{\mathrm{KSO}}}{\gamma_2+\overline{\Gamma}_2}\right]^n\\ &\times\binom{m}{n}-1 , \end{aligned} \tag{A4}$$

$$\begin{aligned} F'_{22}=&\sum_{m=0}^{\infty}\left[\frac{A\overline{\Gamma}_2W_{\mathrm{LO}}}{\gamma_2+\overline{\Gamma}_2}\right]^m\binom{m}{0}-\frac{A\overline{\Gamma}_2}{\gamma_2+B\overline{\Gamma}_2}\\ &+\sum_{n=0}^{\infty}S_n\left[\frac{B\overline{\Gamma}_2W_{\mathrm{KSO}}}{\gamma_2+\overline{\Gamma}_2}\right]^n , \end{aligned} \tag{A5}$$

$$S_n=\sum_{m=n}^{\infty}\left[\frac{A\overline{\Gamma}_2}{\gamma_2+\overline{\Gamma}_2}\right]^{m-n}\binom{m}{n} . \tag{A6}$$

A more useful expression for S_n is obtained by first noting that S_n obeys a recursion relation

$$S_n=\frac{1}{n}\frac{dS_{n-1}}{dC}=\frac{1}{n!}\frac{d^nS_0}{dC^n} , \tag{A7}$$

$$C=\frac{A\overline{\Gamma}_2}{\gamma_2+\overline{\Gamma}_2} . \tag{A8}$$

Starting from $S_0=\sum_{m=0}^{\infty}C^m=(1-C)^{-1}$, where we have used $\binom{m}{0}=1$ the general expression for S_n is obtained

$$S_n=(1-C)^{-(n+1)}=\left[\frac{\gamma_2+\bar{\Gamma}_2}{\gamma_2+B\bar{\Gamma}_2}\right]^{n+1}. \quad \text{(A9)}$$

The relation $A+B=1$ has been used in arriving at Eq. (A8). Using Eq. (A9) in Eq. (A5) the final result is obtained

$$F'_{22}=\sum_{n=1}^{\infty}\left[\frac{A\bar{\Gamma}_2 W_{\rm LO}}{\gamma_2+\bar{\Gamma}_2}\right]^n + \left[\frac{\gamma_2+\bar{\Gamma}_2}{\gamma_2+B\bar{\Gamma}_2}\right]\sum_{n=1}^{\infty}\left[\frac{B\bar{\Gamma}_2 W_{\rm KSO}}{\gamma_2+B\bar{\Gamma}_2}\right]^n. \quad \text{(A10)}$$

This is the form of F'_{22} used for Eqs. (30) and (31). To arrive at Eq. (22) the width of the Lorentzian kernel is set to zero so that $W_{\rm LO}=1$ and the first sum of Eq. (A10) is performed

$$F'_{22}=\frac{1}{\gamma_2+B\bar{\Gamma}_2}\left[A\bar{\Gamma}_2+(\gamma_2+\bar{\Gamma}_2)\times\sum_{n=1}^{\infty}\left[\frac{B\bar{\Gamma}_2}{\gamma_2+B\bar{\Gamma}_2}\right]^n W_{\rm KSO}^2\right]. \quad \text{(A11)}$$

[1] M. J. O'Callaghan and A. C. Gallagher, preceding paper, Phys. Rev. A **39**, 6190 (1989).
[2] P. R. Berman, Adv. At. Mol. Phys. **13**, 57 (1977).
[3] P. R. Berman, Phys. Rep. **43**, 102 (1978).
[4] P. R. Berman, T. W. Mossberg, and S. R. Hartmann, Phys. Rev. A **25**, 2550 (1982).
[5] P. R. Berman, P. F. Liao, and J. E. Bjorkholm, Phys. Rev. A **20**, 2389 (1979).
[6] N. Allard and J. Kielkopf, Rev. Mod. Phys. **54**, 4 (1982).
[7] P. F. Liao, J. E. Bjorkholm, and P. R. Berman, Phys. Rev. A **21**, 1927 (1980).
[8] J. E. Bjorkholm and P. F. Liao, Phys. Rev. A **14**, 751 (1976).
[9] P. F. Liao, J. E. Bjorkholm, and P. R. Berman, Phys. Rev. A **20**, 1489 (1979).
[10] J. E. M. Haverkort, J. P. Woerdman, and P. R. Berman, Phys. Rev. A **36**, 5251 (1987).
[11] D. Veza, J. Lawrenz, and K. Niemax, Z. Phys. D **9**, 135 (1988).
[12] J. Ward, J. Cooper, and E. W. Smith, J. Quant. Spectrosc. Radiat. Transfer **14**, 555 (1974).
[13] K. Blum, *Density Matrix Theory and Applications* (Plenum, New York, 1981).
[14] F. W. Byron and R. W. Fuller, *Mathematics of Classical and Quantum Physics* (Addison-Wesley, Reading, MA, 1970), Vol. 2.
[15] T. Ho and S. Chu, Phys. Rev. A **33**, 3067 (1986).
[16] F. Biraben, E. Cagnac, E. Giacombino, and G. Brynberg, J. Phys. B **10**, 2369 (1977).
[17] E. Giacombino, M. Tawil, P. R. Berman, O. Redi, and H. H. Stroke, Phys. Rev. A **28**, 2555 (1983).
[18] E. E. Nikitin and S. Ya. Umanski, *Theory of Slow Atomic Collisions* (Springer-Verlag, Berlin, 1984).
[19] R. Düren, Adv. At. Mol. Phys. **16**, 55 (1980).
[20] M. J. O'Callaghan, Ph.D. thesis, University of Colorado, 1987.
[21] L. Krause, in *The Excited State in Chemical Physics*, Vol. 28 of *Advances in Chemical Physics*, edited by J. Wm. McGowan (Wiley, New York, 1975).